# A DYNAMICALLY CONSISTENT, MULTIVARIABLE OCEAN CLIMATOLOGY

Ichiro Fukumori, Patrick Heimbach, Rui M. Ponte, and Carl Wunsch

A 20-yr ocean climatology is available that includes all dynamical variables and is consistent with the diversity of data available from the global observation system.

Climatologies, defined as temporal averages of elements of the climate state, have been important in numerous studies. They serve as reference states for inferring changes, as initial conditions in forecasts, and sometimes as the basis of diagnostic dynamical calculations. In an oceanographic context, the most widely employed global climatology has probably been the hydrographic compilation produced initially by Levitus (1982) and its successors as the *World Ocean Atlas* (*WOA*) in its latest form (*WOA13*; Locarnini et al. 2013). They used data from the entire history of physical oceanographic measurements of temperature and salinity as a function of horizontal position and depth. Other global averages include that of Gouretski and Koltermann (2004), from data of the World Ocean Circulation Experiment (WOCE). A number of climatologies of the upper ocean are primarily based on XBT data in the early years (e.g., Ishii et al. 2003; AchutaRao et al. 2007). In related work, but with different emphases, a number of studies of the changing ocean state have been undertaken extending back into the nineteenth century (e.g., Kennedy et al. 2011).

A major issue with most such climatologies and studies based on them has been the very great inhomogeneity with which the ocean has been observed over the years (Fig. 1) and in which the filling of space and time gaps in the record has relied upon sometimes plausible, but generally untestable, statistical assumptions (see, e.g., Boyer et al. 2016; Wunsch 2016). Only temperature—or in a few cases, temperature and salinity—data were available. Furthermore, to our knowledge, no previous extended-time ocean climatology has comprised any variables except the hydrographic ones.

WOCE was designed in large part to produce the first truly global, time-varying estimate of the circulation over approximately a decade, an estimate that would be useful in defining the major climatologically

**AFFILIATIONS:** Fukumori—Jet Propulsion Laboratory, Pasadena, California; Heimbach—The University of Texas at Austin, Austin, Texas; Ponte—Atmospheric and Environmental Research, Inc., Lexington, Massachusetts; Wunsch—Massachusetts Institute of Technology, and Harvard University, Cambridge, Massachusetts
**CORRESPONDING AUTHOR:** Carl Wunsch, carl.wunsch@gmail.com

*The abstract for this article can be found in this issue, following the table of contents.*
DOI:10.1175/BAMS-D-17-0213.1

In final form 12 April 2018

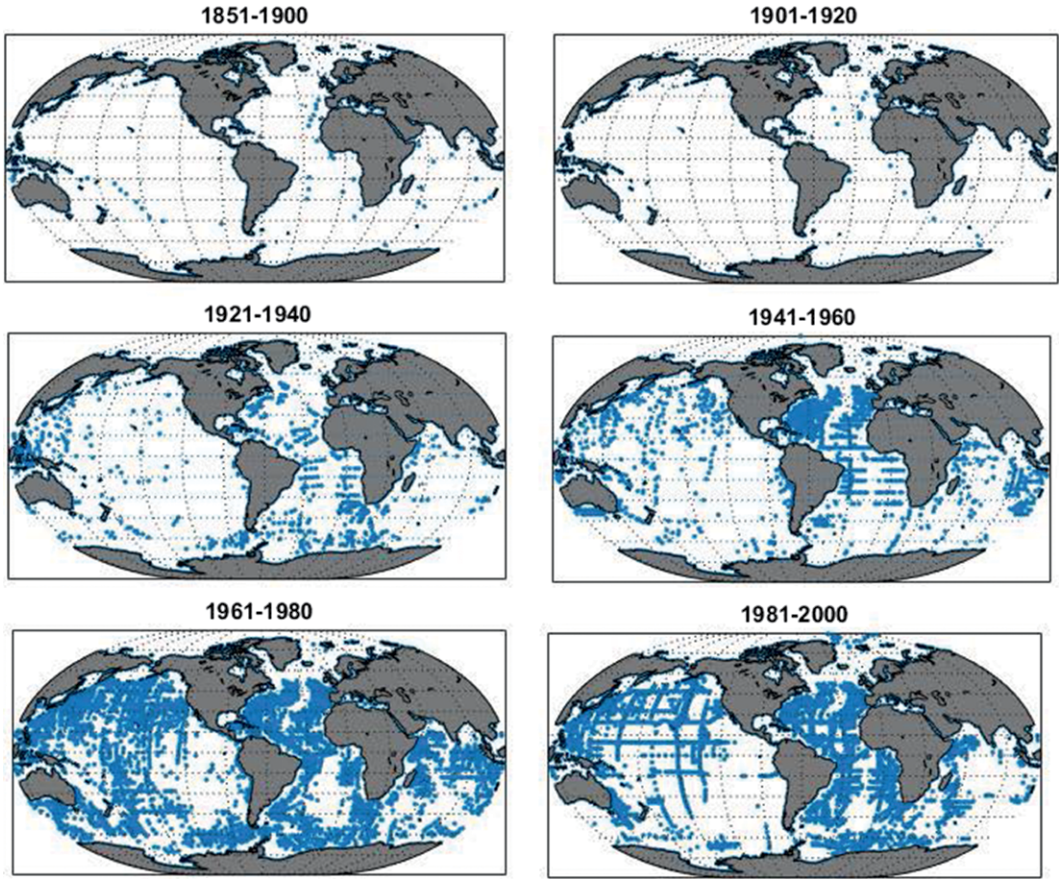


**Fig. 1. Hydrographic measurements reaching at least 3,600 m between 1851 and 1900, and then in 20-yr increments to 2000 (from *WOA*). See Wunsch (2016) for corresponding data distributions to 2,000 m. Early years have a North Atlantic bias, and all years have seasonal biases (not shown) toward low latitudes in winter. Although crude spatial averages could have been formed as early as 1900, even in later decades their accuracy would have been poor. In some cases, shallow topographic features, such as the midocean ridges, are apparent as blank spaces (e.g., the North Atlantic, 1941–60).**

important ocean elements (see Siedler et al. 2013). Until recently, even the best inverse calculations (e.g., Ganachaud and Wunsch 2000; Lumpkin and Speer 2007) were forced to treat quasi-synoptic sections distributed globally over decades as though they represented a consistent time average or, paradoxically, as a snapshot. Such assumptions ultimately are not tenable in a rapidly varying oceanic flow. The Estimating the Circulation and Climate of the Ocean (ECCO) project was formed to address this goal using both the conventional and newly deploying WOCE observation system, along with the rapidly advancing time-varying general circulation modeling capability (Stammer et al. 2002, 2003). This present paper is intended to introduce another climatology, based on an updated edition (release 3; Fukumori et al. 2017) of the latest version, version 4, of the ECCO ocean state estimate (Forget et al. 2015). The climatology here is focused on the 20-yr period 1994–2013, an interval in which a comparatively homogeneous set of global-scale observations—many extensions of those in WOCE—were obtained so that the zero-order sampling difficulties visible in Fig. 1 are much reduced. The major inhomogeneity in the present climatology stems from the growing availability of Argo floats beginning about 2000 and extending to the present day (Roemmich et al. 2009), but the dominant datasets, including altimetry and CTDs,

**▸ Fig. 3. WOCE section of potential temperature (°C) nominally down 25°W in the Atlantic Ocean, although the ships deviated from that longitude (from Koltermann et al. 2011). Notice the presence of much small-scale structure of several degrees of latitude not present in the 20-yr mean section (Fig. 2). Data used to produce the published WOCE atlas plate were obtained in 1988 and 1989, while additional WOCE data on this line, used in the state estimate, were measured during the specific climatology interval. Differences from those observations are a part of the data misfit discussion and are dominated by the small scales (not shown).**

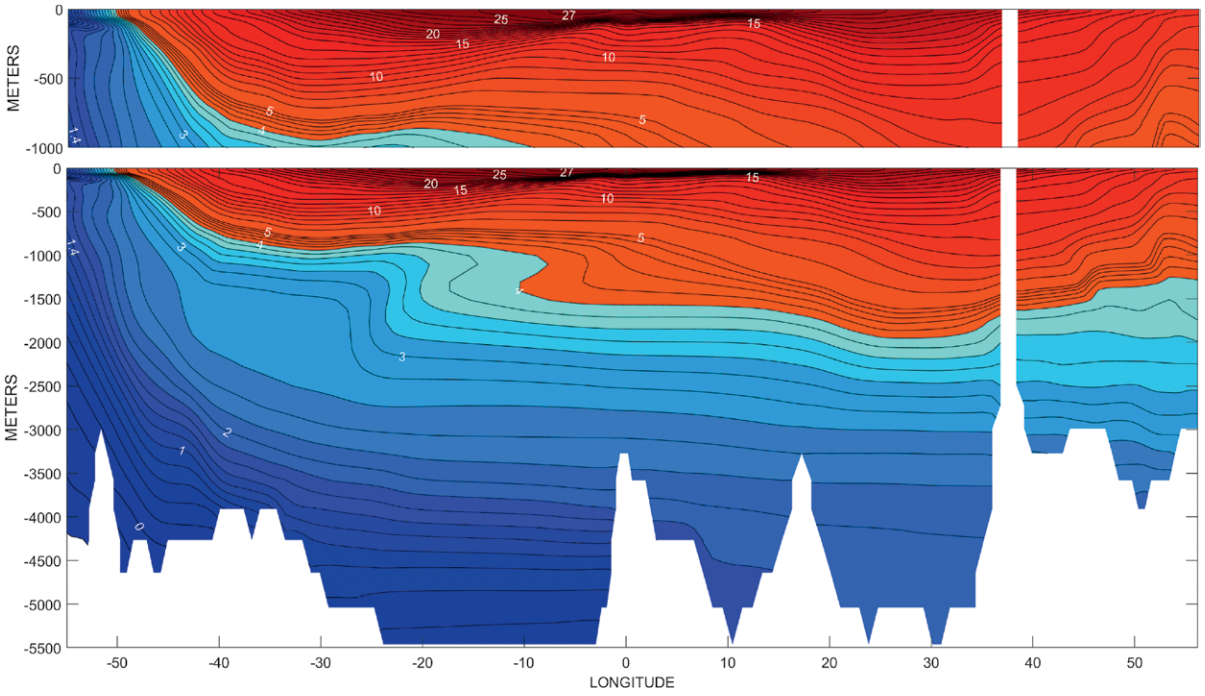


**Fig. 2. Twenty-year mean section of potential temperature (°C) down 25°W in the Atlantic Ocean. Region in white is bathymetry. The section is smoother than any quasi-synoptic section would be, although considerable structure remains despite the averaging time. Compare to Fig. 3 showing quasi-synoptic shipboard measurements from the late 1980s. Color coding is similar but not identical.**

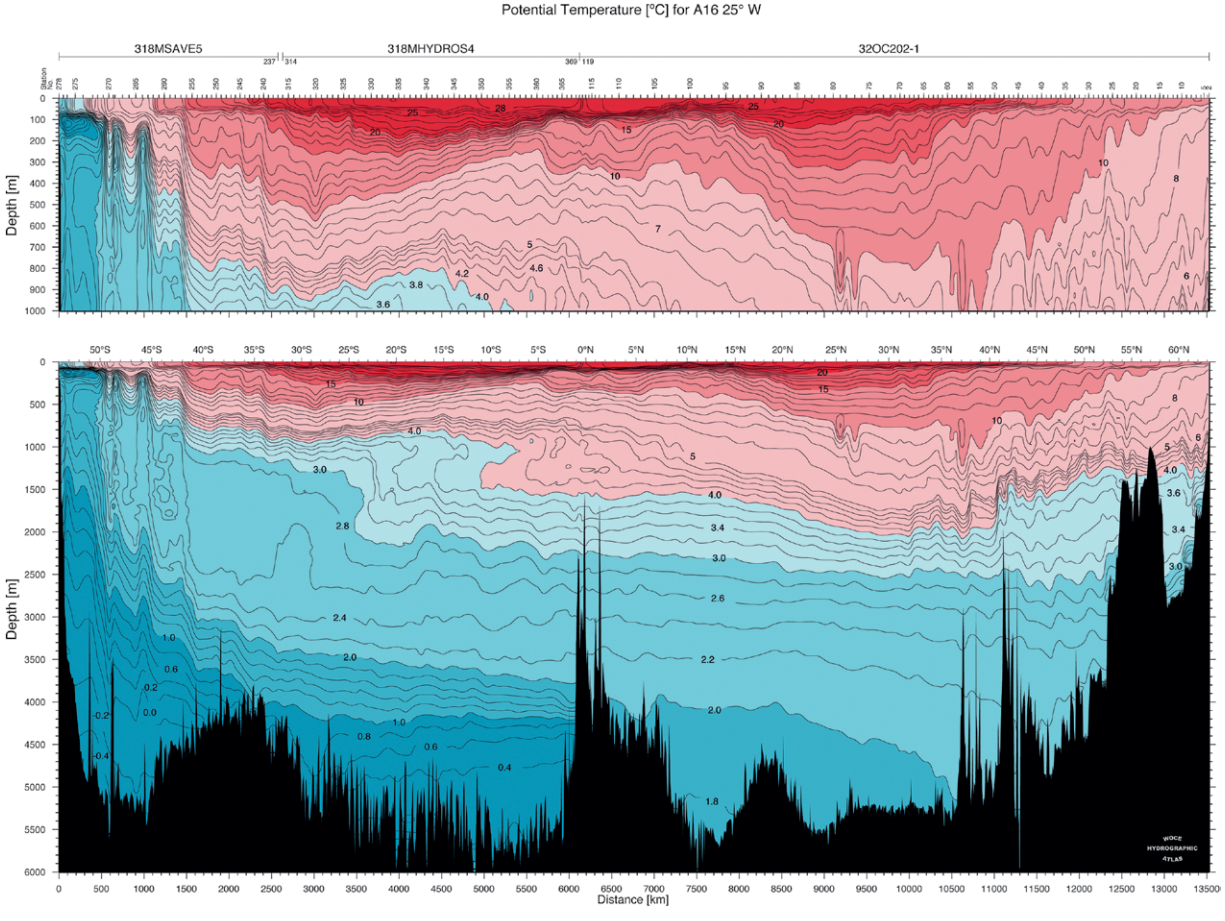

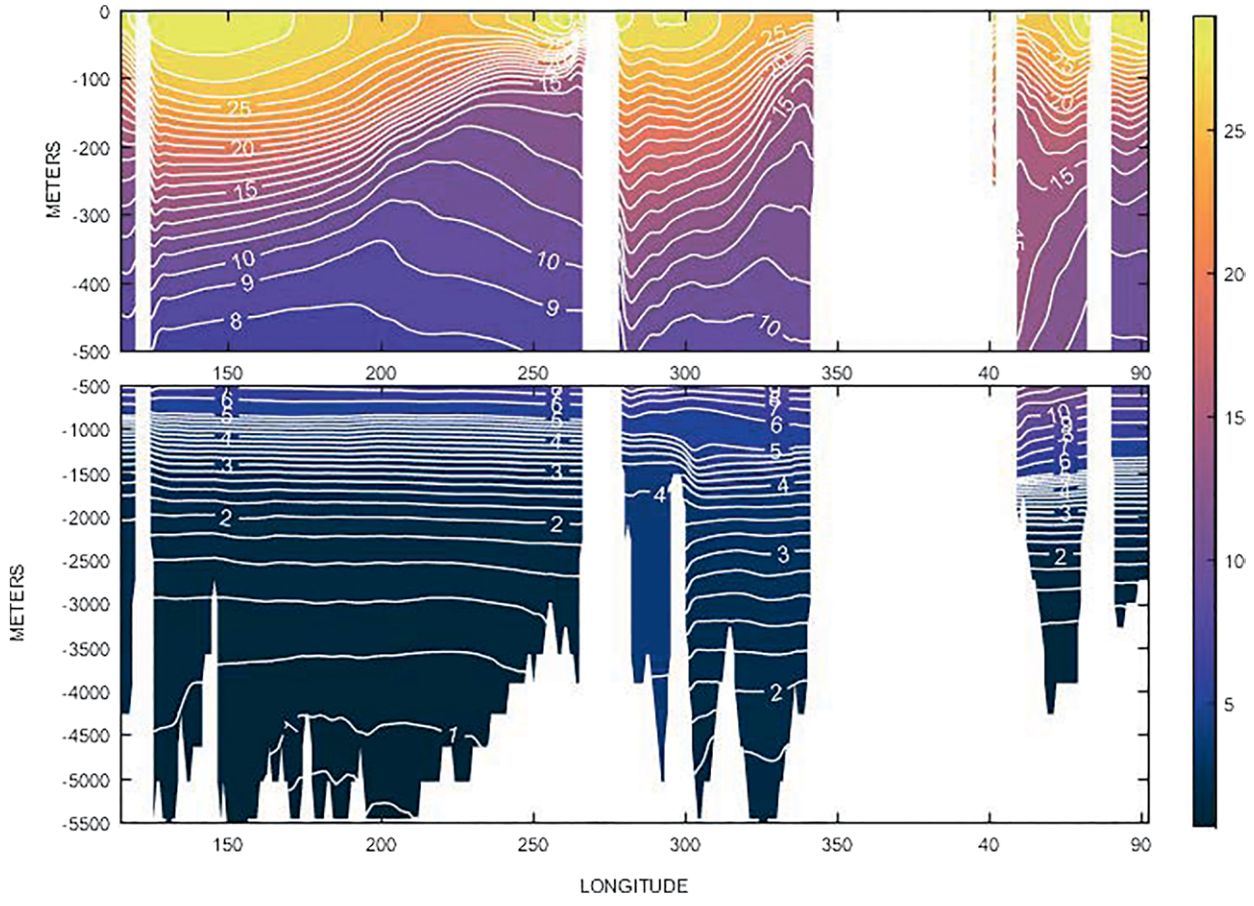


**Fig. 4. Twenty-year mean potential temperature (°C) in all three oceans along 14°N. Both Atlantic and Pacific Oceans display the expected eastward tilt of the thermocline and with nearly flat isotherms at depth except where major topographic features are encountered.**

are nearly homogeneous over the entire interval and, in particular, do not display the Northern Hemisphere–Southern Hemisphere asymmetries plaguing earlier climatologies (e.g., Abraham et al. 2013). Use of dynamics further reduces the effects of the remaining inhomogeneities.[1]

The word *climatology* originally referred specifically to averages of weather (*Oxford English Dictionary*, 3rd ed., s.v. "climate"), now sometimes requiring 30-yr intervals—a duration determined by the behavior of weather statistics. Here, following many previous efforts, the expression is extended to the ocean, and further extended to include a description of the dominant time changes hidden within the average. Because of the very long time scales present in oceanic fluctuations, a mean comparable there to a 30-yr atmospheric average would probably require hundreds of years. A 20-yr ocean average does suppress much high-frequency variability and is a useful reference state.

Essentially all of the available hydrographic data are used, including CTD hydrography (Talley et al. 2016); measurements from elephant seals (Roquet et al. 2013), XBTs, and Argo temperature and salinity profiles (Riser et al. 2016); and sea surface temperature products (Reynolds and Smith 1994, 1995). But *in addition,* the complete altimetric record, which begins in 1992, is employed (e.g., Fu and Cazenave 2001) and a mean topography constructed from it (Andersen et al. 2015), as are the Gravity Recovery and Climate Experiment (GRACE) satellite gravity measurements (Quinn and Ponte 2008; Watkins et al. 2015) and the available a priori estimates of the meteorological forcing during the climatological interval (Dee et al. 2011, 2014). A nearly complete list is contained in Table 21.2 of Wunsch and Heimbach (2013) with details of about 11 generic data types. Fukumori et al. (2017) provide full details of data sources, processing, and uncertainty weights.

[1] The estimation interval begins in 1992 and extends nearly to the present time. Data observed prior to 1992 appear only tangentially in constructing first-estimate adjustable initial conditions from previous climatologies.

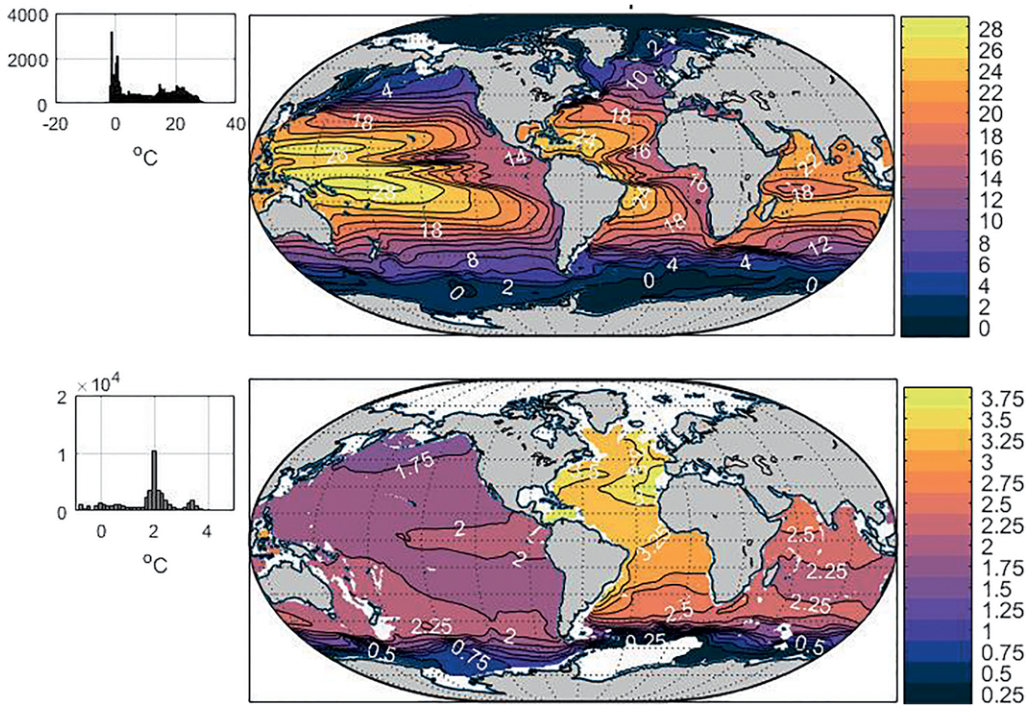


**Fig. 5. (top) Twenty-year average potential temperature at 105 m (°C). Inset shows the histogram of values at this depth. Dominant features are the subtropical gyres in all oceans and the relatively very cold water in the Southern Ocean. (bottom) Twenty-year average temperature at 2,084 m (°C). Color saturates at 3.9°C with outlier maxima occurring in the Mediterranean and Gulf of Mexico, where the deep-water resolution is inadequate for the topography. The relative warmth of the North Atlantic Ocean is prominent.**

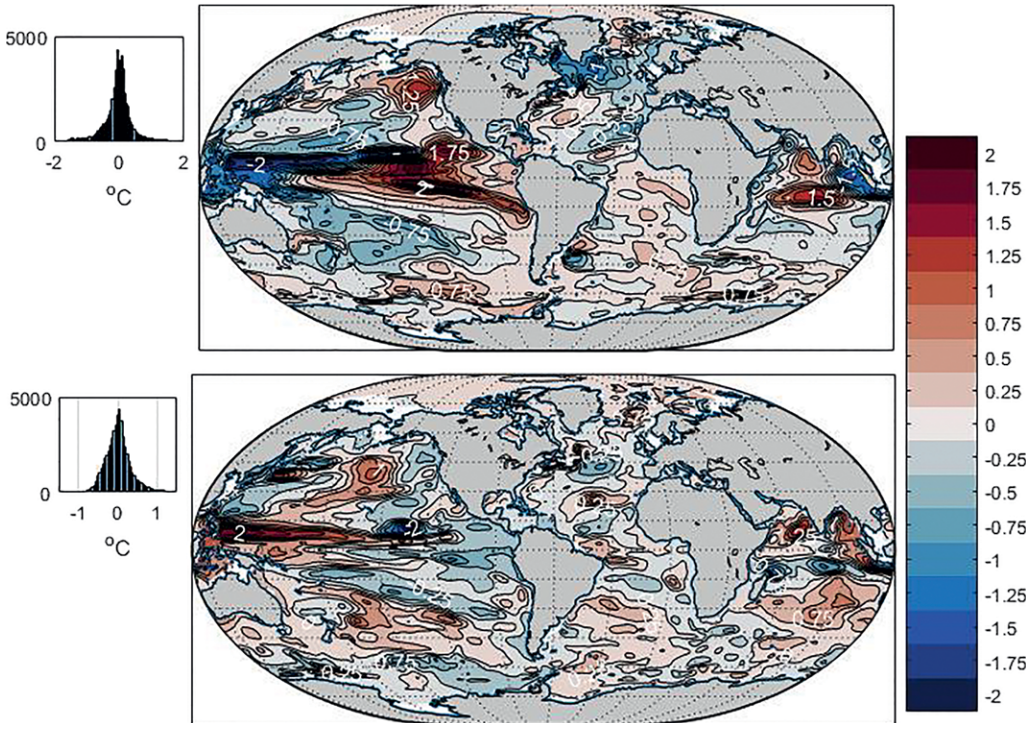


**Fig. 6. (top) Anomaly of temperature (°C) in 1994 relative to the 20-yr mean at 105 m. The complex spatial structure emphasizes the need for approximately uniformly distributed global measurements if accurate basin or global averages are sought. (bottom) Annual mean anomaly of temperature (°C) at 105 m in 2013, 20 years after that in the top panel.**

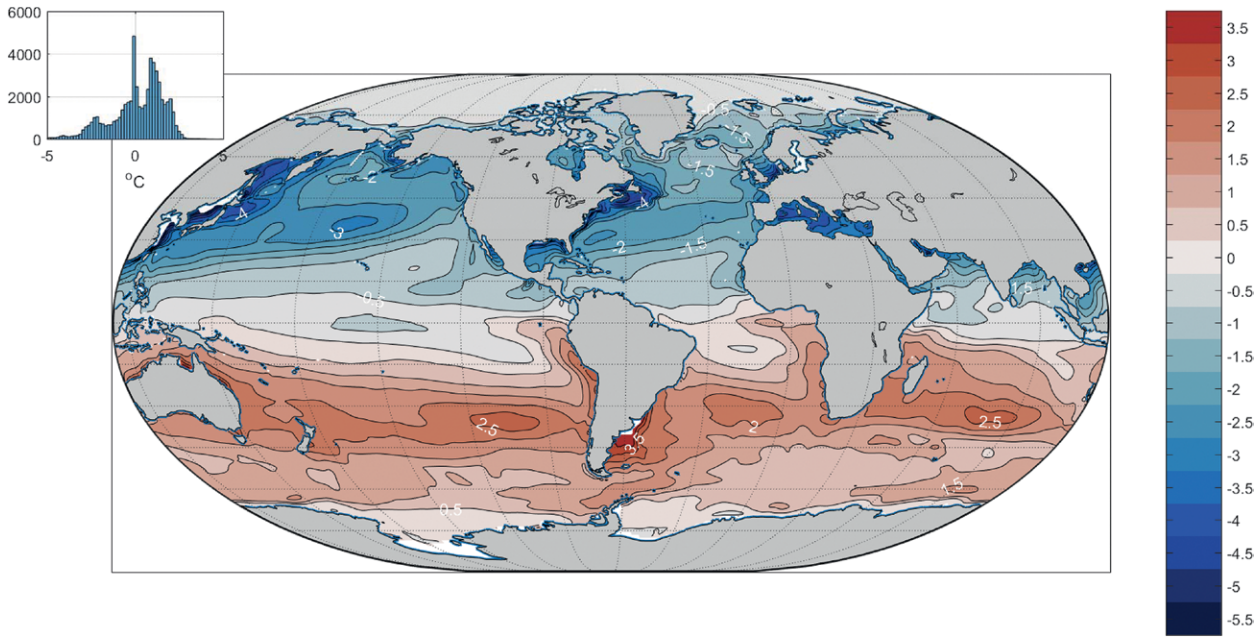


**Fig. 7. Example of a 20-yr average seasonal (DJF) mean 5-m temperature (°C) anomaly relative to the 20-yr mean. The main feature is the interhemispheric antisymmetry with the conventional larger amplitudes in the northern region. Southern Hemisphere boundary currents are conspicuous.**

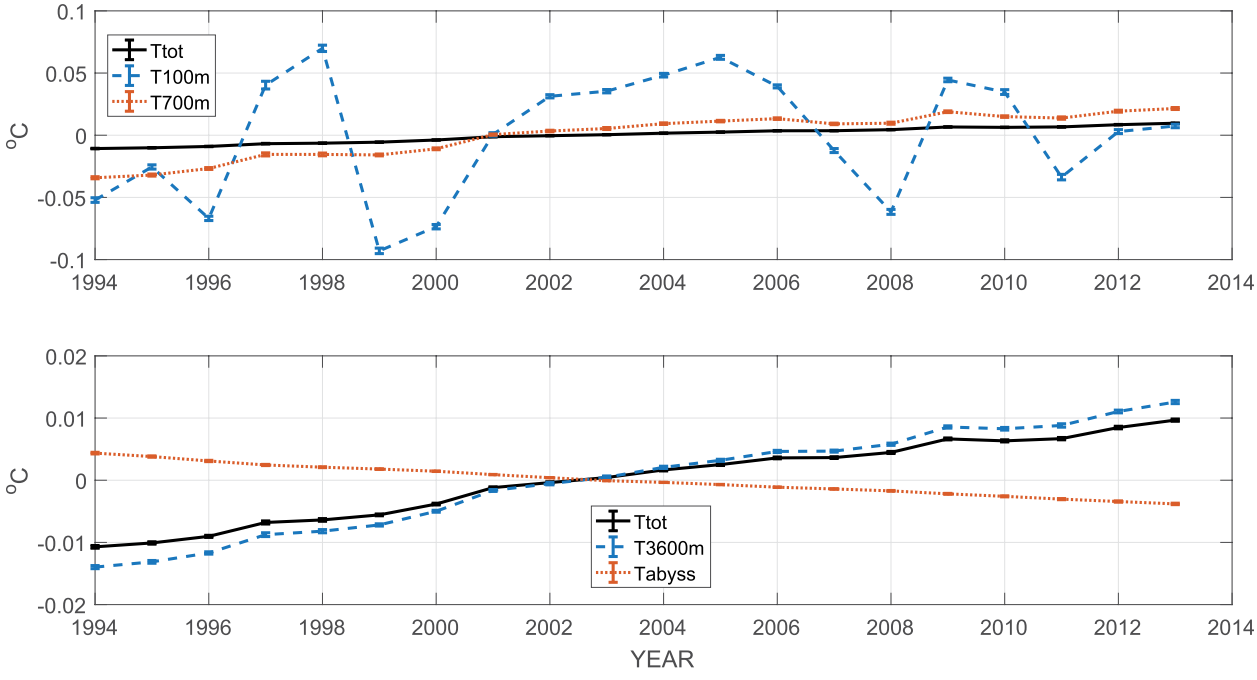


**Fig. 8. Volume-weighted temperature change (°C) by year. (top) Average to 100 m, 700 m, and the total (Ttot). (bottom) The averages to 3,600 m, the total, and the abyssal layer below 3,600 m, which shows net cooling. Formal (stochastic component) error bars are for the annual volume mean as computed from a bootstrap method as described by Wunsch (2018). The deep cooling is discussed by Wunsch and Heimbach (2014) and rationalized by Gebbie and Huybers (2017, manuscript submitted to *Science*).**

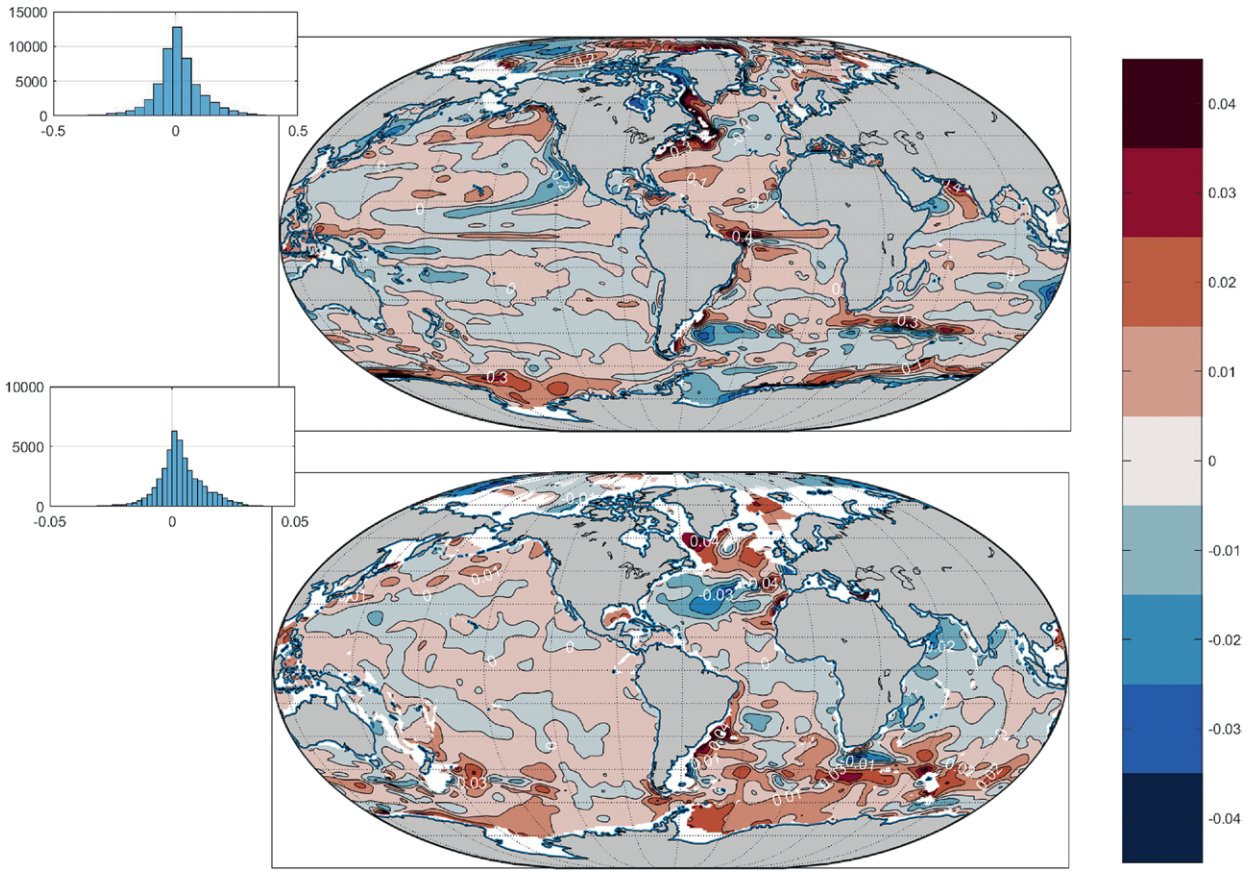


**Fig. 9. (top) Misfit of the state estimate to the Gouretski and Koltermann (2004) salinity climatology (practical salinity scale) averaged over 20 years at 105 m. Histogram inset shows the distribution of values, which is unimodal about 0 and close to Gaussian. Some isolated outliers are omitted. Major deviations are primarily associated with marginally resolved coastal and other jetlike currents, such as the Agulhas retroflected flow. (bottom) As in (top), but at 2,084 m. Although not formally tested, the residuals have a visual resemblance to a stochastic field with regional variations; see the discussion in Wunsch (2018). Available fields permit computation of misfits to all observations used in the state estimate over months, years, seasons, and the duration and position including, where appropriate, as functions of depth.**

*Combining data and dynamics.* To combine the diverse datasets, including the surface forcing fields, a least squares fit is made of a state-of-the-art ocean/sea ice general circulation model (Forget et al. 2015; cf. Marshall et al. 1997; Adcroft et al. 2004; Wunsch and Heimbach 2007, 2013; Wunsch et al. 2009). Fitting is achieved by adjustments of model initial conditions, mixing coefficients, and meteorological exchange fields. As is done in conventional least squares fitting, all data and adjustments are weighted by the best-available estimates of their uncertainties—written as error variances or covariances. Because of the huge dimension of the resulting calculation, the fit is carried out by numerical iteration using Lagrange multipliers (adjoint or dual solutions; see Wunsch and Heimbach 2013; Forget et al. 2015). The Lagrange multipliers enforce the model, which includes numerous adjustable parameters.

The state estimate over the 20 years is then obtained from the *free-running* ECCO configuration of the Massachusetts Institute of Technology General Circulation Model (MITgcm), started from the adjusted initial conditions and mixing coefficients, and subject to the adjusted meteorological forcing fields, which render the model state generally consistent with the observations within estimated uncertainties. The time step of the model is 1 h over the interval 1992–2015 with only the shorter interval 1994–2013 used in the present climatology. As the product of a GCM, by construction generally reproducing within error estimates all of the data used, the state estimate permits calculation of ocean properties beyond what is directly observed and includes values of the three-dimensional time-varying velocity field, the surface elevation and its changes, bottom pressure, and ice cover, as well as the parameters representing the

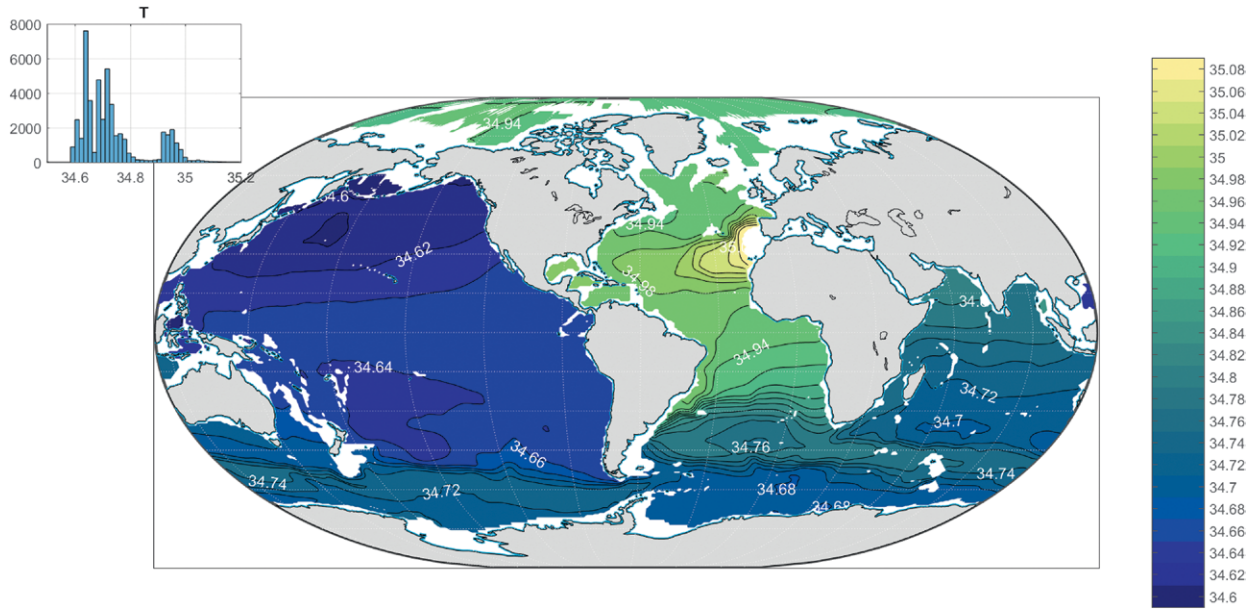


**Fig. 10. Twenty-year average salinity (practical salinity scale) at 2,084 m. Excess values in the North Atlantic and the extreme of the Mediterranean Sea outflow (Mediterranean Sea values are truncated here) are visible. The relatively saline Atlantic Ocean is apparent, mimicking the thermal differences seen in Fig. 8.**

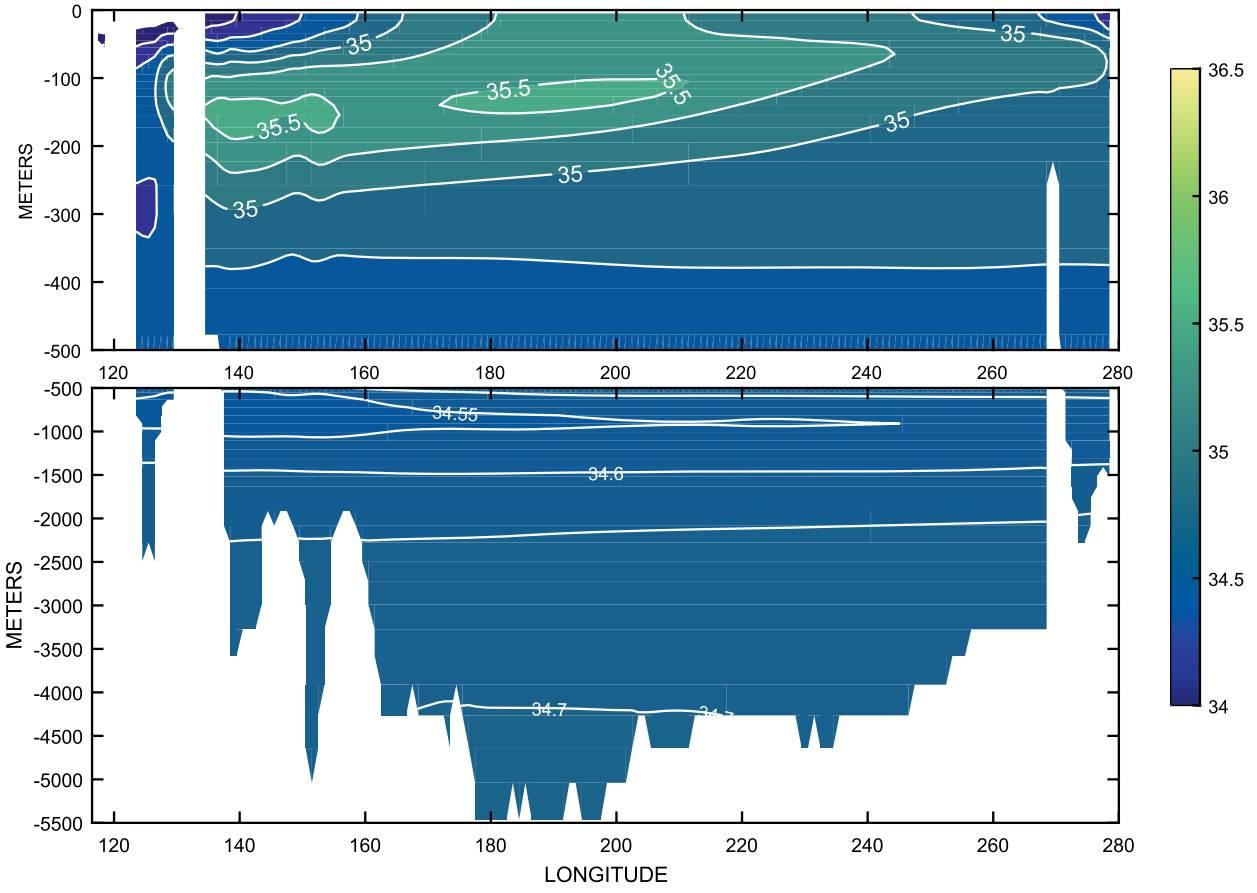


**Fig. 11. Twenty-year average salinity (practical salinity scale), in a zonal section along the equator in the Pacific Ocean. Note extra contours below 500 m. The steep upward slope of the halocline to the east is part of the discussion of time-mean equatorial dynamics.**

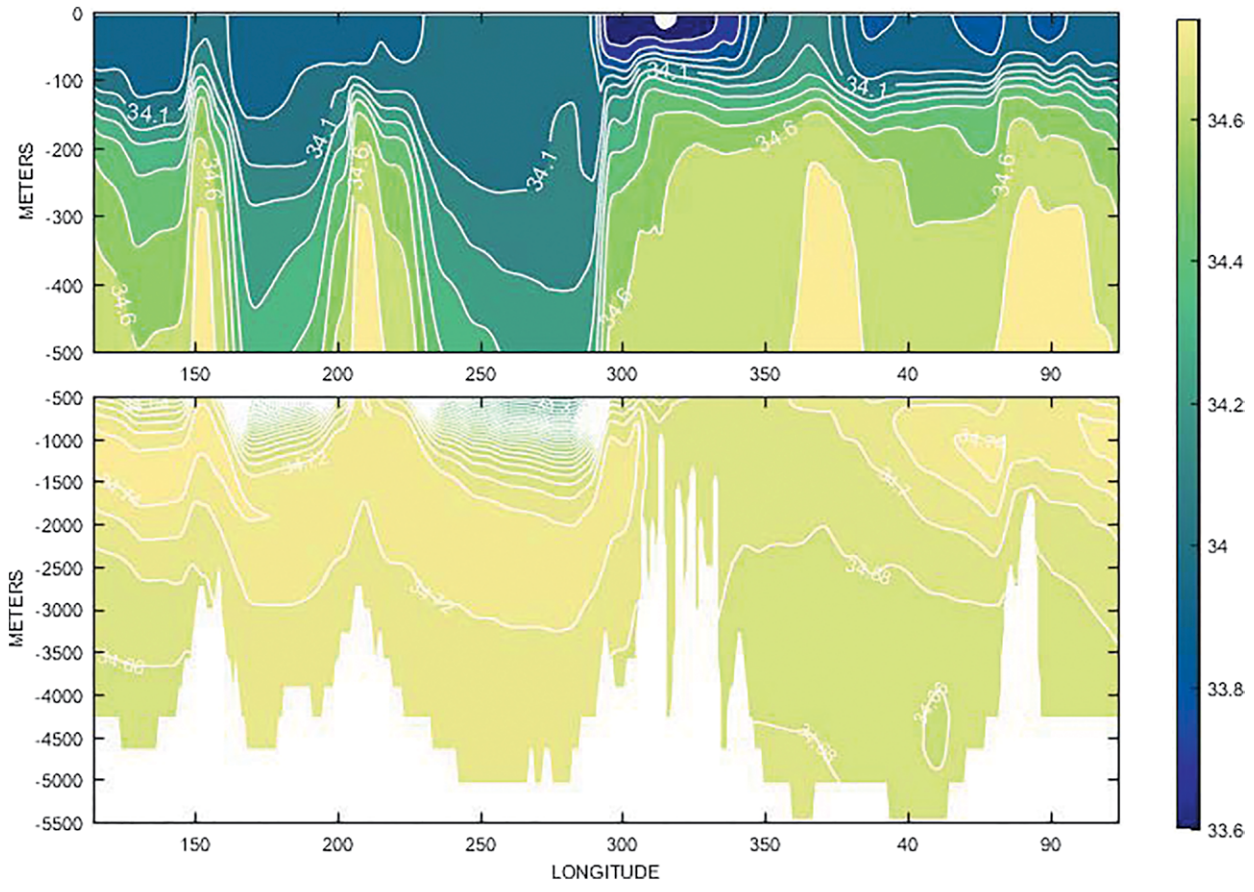


**Fig. 12. Twenty-year mean salinity (practical salinity scale) in a zonal section through the Drake Passage (60°S) with a complex structure as seen also in temperature (not shown here; see ECCO Consortium 2017a) and producing a similarly complex zonally varying temperature–salinity relationship in the Southern Ocean.**

nonresolved eddy mixing via the bolus transport of Gent and McWilliams (1990) and related schemes. Also included are the misfit fields to the different datasets used as constraints. As fitting iterations continue, new data are added, the duration increases, and the model continues to develop, the climatology changes, although at this stage future adjustments are expected to be quantitatively small in most aspects.

Differences from existing ocean climatologies. We make no claim that the ECCO, version 4, state estimate is "better" than existing ones, because such a claim depends directly upon the intended use. Anyone interested in oceanic changes prior to 1992 must look elsewhere. As reference fields, the ECCO results do provide graphic displays of the complexity of both time-mean and spatial variations, including changes in the full water column, as well as estimates of the range of adjustments necessary for meteorological fields required to be consistent with oceanic observations.

In specific contrast to what are usually called "reanalysis products," the state estimate satisfies all of the conventional conservation requirements for any dynamically consistent climate component, including energy, heat, freshwater, vorticity—up to the accuracy of the general circulation model equations. Although considerable extra computation is required to obtain dynamically consistent solutions, no artificial interior sources and sinks appear (Wunsch and Heimbach 2013; Stammer et al. 2016), thus permitting study of changes in energy, heat content, and so forth. See Bengtsson et al. (2004) for a discussion of the difficulties in using reanalysis climatologies.

In ECCO, diverse datasets are brought to bear on all of the elements of the state estimate. All observations have limits of sampling, random and bias errors, and finite duration. So, for example, even the revolutionary Argo datasets alone fail to adequately depict important physical processes (e.g., Evans et al. 2017). The state estimate provides, in addition to the directly measured variables, all those required by or computable from a free-running general circulation model.

A quantitative and explanatory comparison of the numerous existing attempts at forming oceanic

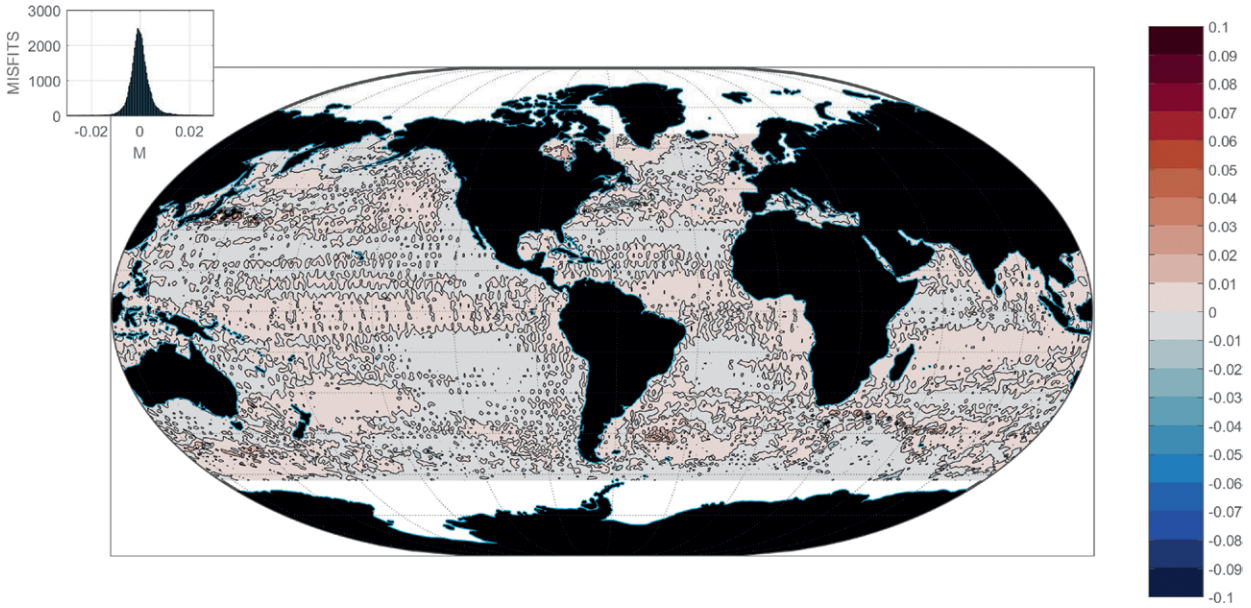


**Fig. 13. Average misfit (m) over 20 years of the state-estimated values of $\eta$ and that measured by the suite of Ocean Topography Experiment (TOPEX)/Poseidon–Jason altimeters. Based upon the average of the monthly misfits in the generally ice-free region. Weighting operators were chosen, so small-scale features are ignored in the least squares fitting, as they are dominated by geoid error and mesoscale features. Unimodality-about-zero character of the residuals is clear, but large-scale patterns suggest residual systematic errors in the altimeter data or in the model on the order of 2 cm. Complex detail of the zero contour, which dominates the plot, is consistent with a zero-mean, nearly random, residual. As with the salinity misfit in Fig. 13, these fields are computable over arbitrary data intervals within the 20-yr climatology time span.**

climatologies would take us very far afield and would be limited to direct measurements. As one example, however, using an earlier ECCO product, Forget (2010, his Fig. 14) showed that the *WOA* produced unphysically large (compared with meteorological estimates) flux divergences of heat and freshwater. By construction, the ECCO-adjusted atmospheric exchange estimates are consistent with the ocean circulation. Another example can be found in Evans et al. (2017, particularly their Figs. 4, 5), who compared the ECCO, version 4, North Atlantic water masses with an Argo-alone dataset and discussed reasons for their differences.

**BASIC FIELDS.** A description of the time-varying three-dimensional global oceanic state and its interpretation is a forbidding undertaking. What is intended here is to call attention to the availability of fields useful for a great variety of purposes, to explain how to obtain the fields in simple ways, and to invite the use and critique of the result by the wider community. A more elaborate pictorial description has been posted with links from the ECCO website, at the present moment in two distinct parts. Part 1 (ECCO Consortium 2017a) is devoted to the hydrographic and derived fields, such as surface elevation and mixed layer depths. Part 2 (ECCO Consortium 2017b) focuses on the flow fields and meteorological variables. Intended for later parts are discussions of the adjoint model (the dual model of Lagrange multipliers and sensitivities) and an analysis of the uncertainties. Fukumori et al. (2017) described the major changes from earlier ECCO estimates. Numerous discussions of various fields, beyond what we have space for here —such as bottom pressure; regional and global sea level; air–sea transfers, etc.; means and variations—are listed in the references of these other papers.

In the spirit of a climatology, and in the interests of an easily workable volume of numbers, the discussion here is limited to the 20-yr average, the 20-yr average months (January, February, …), the 20-yr average seasonal cycle [June–August (JJA), etc.], and the yearly averages (1994, 1995, …, etc.).

Of necessity, only a few representative fields are shown here and with a few applications chosen to portray some of the more interesting or useful products. In an ocean state with 50 levels in the vertical, and strong geographical variability, each depth and region is at least slightly different from any other, and a complete depiction and rationalization is not possible within normal journal space limits. Additional fields and products can be seen in the online documents or in the many references given there. None

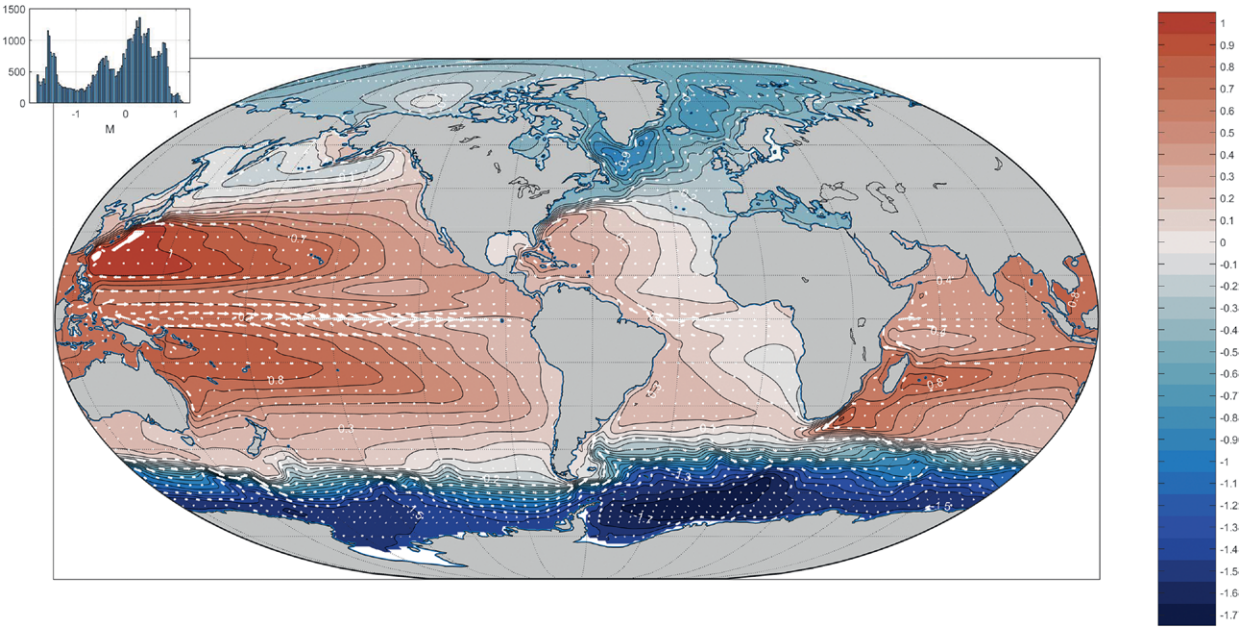


**Fig. 14. Twenty-year mean dynamic topography (m) from the model mean sea surface elevation. Values in ice-covered regions are corrected for the ice load and differ there from equivalent sea level. Offsetting the entire surface by a constant would have no observable dynamical consequences. Compare to Maximenko et al. (2009) and Knudsen et al. (2011). Inset shows the histogram of values about the mean. The overall range is about 3 m. Arrows show the flow field, which is dominantly geostrophic, at 105-m depth.**

of these results should be regarded as definitive; they are presented chiefly an invitation to any interested scientist to recompute them as desired with different assumptions, averaging, etc.

The model native grid is shown in Forget et al. (2015). As Forget et al. (2015) discuss, at high northern latitudes a distorted grid is used to avoid the polar singularity. The complexity of the high-latitude gridding is one of the motivations for producing this easier-to-use climatology. An interpolation to a simple latitude–longitude grid has been used here for mapping purposes. A display of fields on the native grid, including high latitudes, can be seen in the various references and on the ECCO website. A specific high-northern-latitude version of the state estimate and its corresponding climatology is in preparation (Nguyen et al. 2017). Elsewhere, longitudes are uniformly spaced at 1° and latitudes telescope toward the equator (where it is 0.41°) and decrease northward from 1° to about 1/2° at 57°. Over most of the oceanic domain, grid latitude distances maintain nearly constant grid areas.

*Hydrography.* Potential temperature. An example of a 20-yr average hydrographic section is shown in Fig. 2 and can be compared to the nearby quasi-synoptic WOCE section in Fig. 3. The gross structures are identical, but the average field is considerably smoother than the WOCE section. Because much of the data used to produce the WOCE atlases (http://woceatlas.ucsd.edu/; and see Schlitzer 2018) were also used in the state estimate, large-scale gross structures in the ocean circulation can be seen readily in the various WOCE atlases and so are not reproduced here. Figure 4 shows one example of a global thermal section at 14°N, and Fig. 5 shows examples of temperatures at fixed depth levels [color coding here often follows that suggested by Thyng et al. (2016) both to accommodate color-blind readers and to avoid inadvertent emphasis of some features]. These and other fields are time averages consistent with the time-mean flow and meteorological fields displayed below. In many cases, a histogram of values is shown as an inset. Inevitable outliers (usually within topographically complex areas beyond the model resolution) are omitted in most plots.

Time dependence. Elements of the fluid ocean change constantly. As examples, Fig. 6 shows the estimated annual mean anomalies at 105 m for two different years. Figure 7 is the 20-yr average seasonal anomaly in December–February (DJF) at 5 m. All charts, despite the 20-yr averaging, retain a spatial complexity that emphasizes the challenges of forming adequately accurate global averages. The annual anomalies permit calculation of the changing heat content of

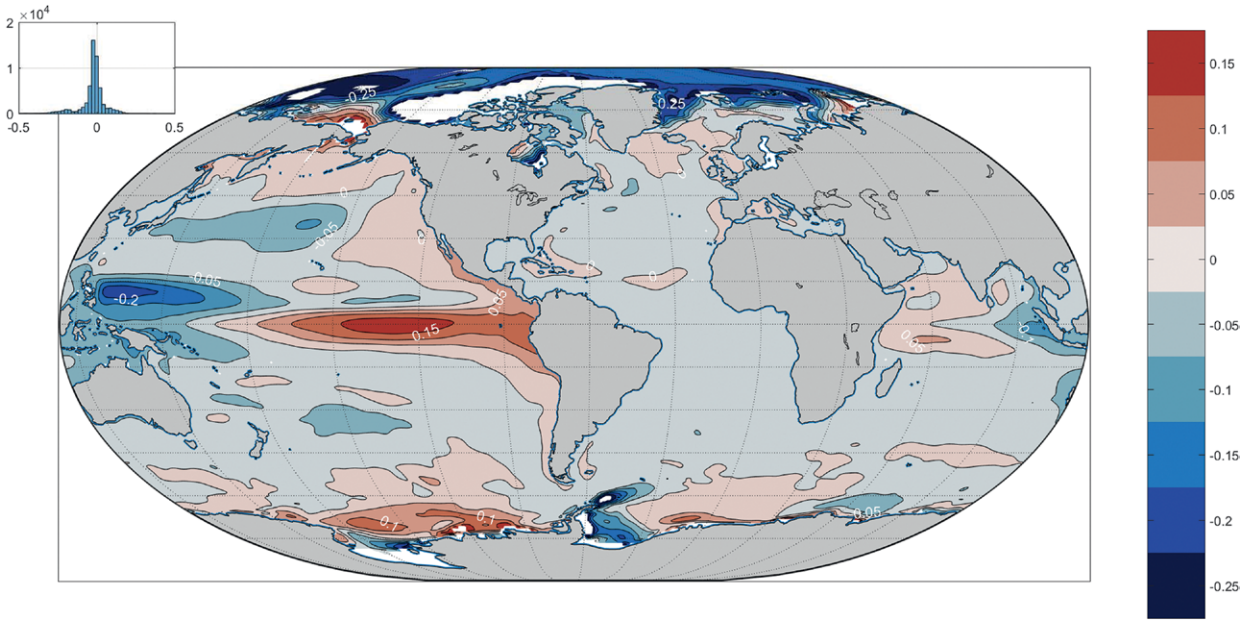


**Fig. 15. Average of the anomaly of $\eta$ (m) during an El Niño year (1997) with the expected elevation excess in the eastern Pacific Ocean. Structure elsewhere becomes part of the discussion of the global elements of ENSO.**

the ocean over 20 years, shown as the corresponding temperature changes at different levels in Fig. 8. Error estimates are described briefly below and are obtained from bootstrap estimates derived from the spatial distributions of temperature with systematic effects first having been suppressed. Upper levels are noisy, while the deeper ones can be interpreted as showing simple linear trends. These and other products become part of the discussion of the oceanic heat uptake, the putative slowdown in atmospheric warming ("hiatuses"), and others (see Wunsch and Heimbach 2014; Medhaug et al. 2017; Liang et al. 2017b).

Salinity. As a least squares estimate, the ECCO state leaves explicitly computed misfits by month, year, and on the average. As an example, Fig. 9 shows the gridded 20-yr mean misfit to the salinity data at 5 and 2,084 m. Apart from outliers in the Labrador Sea and other shallow regions (see, e.g., Fenty and Heimbach 2013), the observations are generally within 0.5 on the practical salinity scale over most of the ocean. The implications of regional misfits for overall behavior of the state estimate would apply to any model calculation, whether constrained or not. In the present situation, the Lagrange multipliers (adjoint or dual solution) are available for a sensitivity determination, but their use is not pursued here.

The time-average salinity field at one depth is shown in Fig. 10. The histogram inset shows a multimodal distribution of values. In Figs. 11 and 12 two 20-yr average zonal sections of salinity are displayed along the equator and through the Drake Passage, respectively. A great deal of structure remains even after 20 years of averaging.

*Pressure and flow fields.* Surface elevation. Surface elevation $\eta(\theta,\lambda,t)$ relative to an estimated geoid is partially, but not completely, determined by the altimetric data: the state estimate is simultaneously being fit to meteorological forcing; the thermal, salinity, and ice-cover fields; and any other data (e.g., gravity and altimeter height changes) that are present. A full determination of which elements of which observations are controlling the field depends upon the adjoint sensitivity of estimated $\eta$ to each of these datasets. Altimetric records are the only ones nearly uniform and global over the entire 20 years, and the 20-yr average misfit to the time-varying altimetric measurement of $\eta$ is shown in Fig. 13. Apart from outliers that have been suppressed in the charts, the misfits are generally within 10 cm overall, are highest at high latitudes, and are showing some residual structures in the tropics. Misfits associated with the moving western boundary currents also appear.

Explanations of residual misfits involve discussion of possible improvement by further iteration of the least squares minimization; model errors, including resolution issues and inadequate parameterization; and incomplete understanding of the observational errors. These will usually be functions of geographical position and possibly time, including seasonal effects.

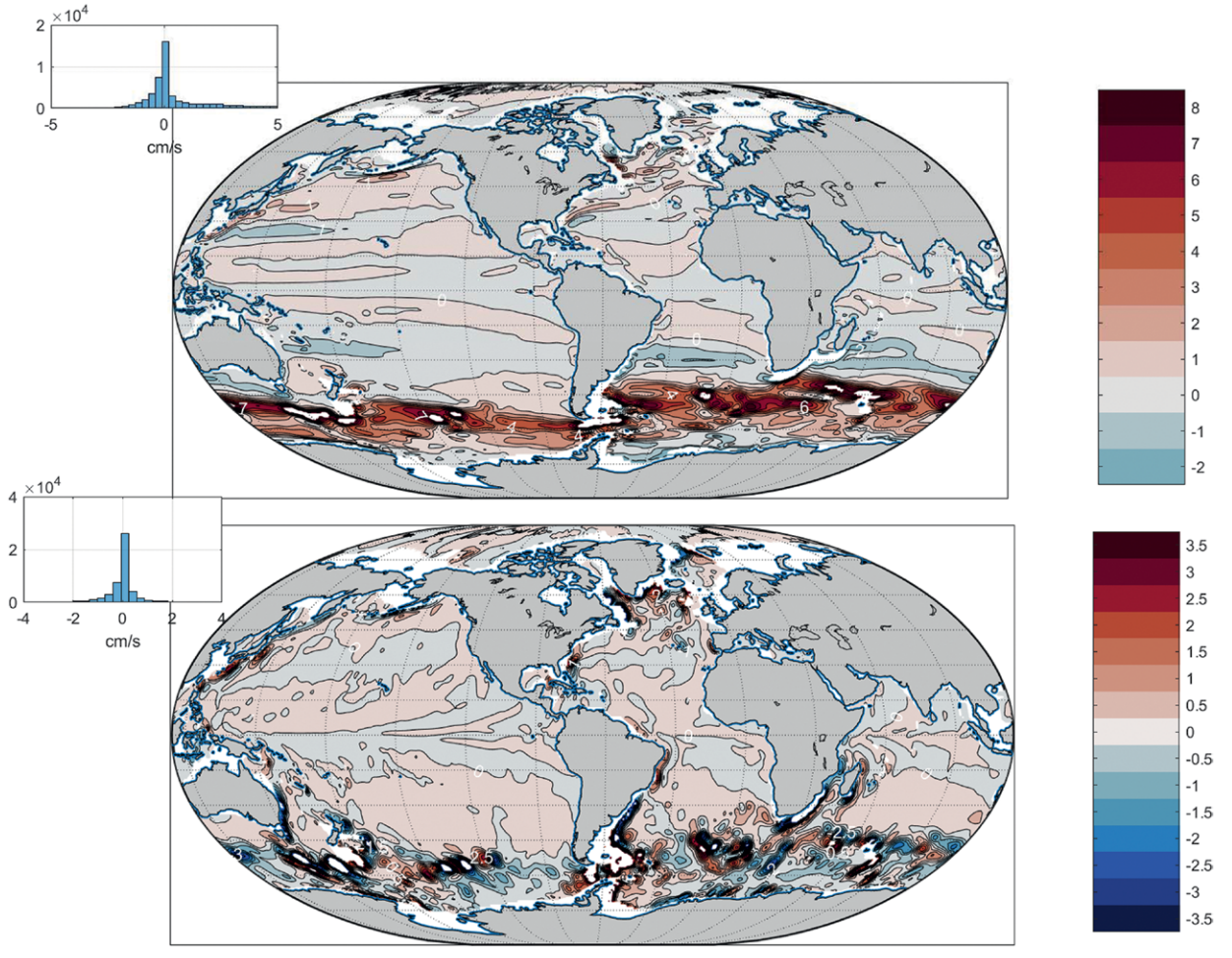


**Fig. 16. Twenty-year average horizontal flow (cm s$^{-1}$) at 1,000 m. (top) Zonal component *u* and (bottom) meridional component *v*. Note the different color scales. Compare to Ollitrault and Colin de Verdière (2014).**

Elevation and pressure. The time-average dynamic topography, relative to the GRACE geoid, appears in Fig. 14 and again shows the classical gyres. Dynamic topography differs from $\eta$ in the ice-covered region where the pressure load is accounted for. The anomaly of $\eta$ in 1997 appears in Fig. 15 and is the anomaly of dynamic topography in the ice-free regions.

Hydrostatic pressure fields, including bottom values, are also available; see, for example, Piecuch et al. (2015). Temporal variations are discussed by Forget and Ponte (2015) and Sonnewald et al. (2018).

Flow fields. The 20-yr average horizontal components of Eulerian velocity ($u$, $v$) are displayed in Fig. 14 at 105 m and in Fig. 16 at 1,000 m. These include both the geostrophic and ageostrophic components. The 1,000-m flows are readily compared—for example, to the results of Ollitrault and Colin de Verdière (2014) from Argo trajectories alone—and which are noisier.

A zonal flow anomaly in 1995 in the Drake Passage is shown in Fig. 17. Annual average velocity anomalies are very small, but between 1994 and 2013 (not shown) they produce a transport variability between −5 and +3 Sv (1 Sv ≡ $10^6$ m$^3$ s$^{-1}$). Integration across a complex velocity structure is required to obtain the transports.

The Eulerian vertical velocity $w$ is a crucial element in the oceanic general circulation, especially in the vorticity balance. Figure 18 displays the 20-yr mean $w$ pattern at 105 m, a rough equivalent to the Ekman depth. Sign changes correspond to the classical gyre circulation as well as to the intense equatorial and coastal upwelling phenomena. At great depths (not shown), the pattern rapidly becomes complex beyond a simple verbal description, and particularly as topographic features are approached from above. See Liang et al. (2017a) for a discussion including that of the bolus velocity $w_b$ and its sum with $w$.

*Meteorological values.* Meteorological forcing variables of wind, surface air temperature, specific humidity, precipitation, and radiative fluxes from the European Centre for Medium-Range Weather Forecasts

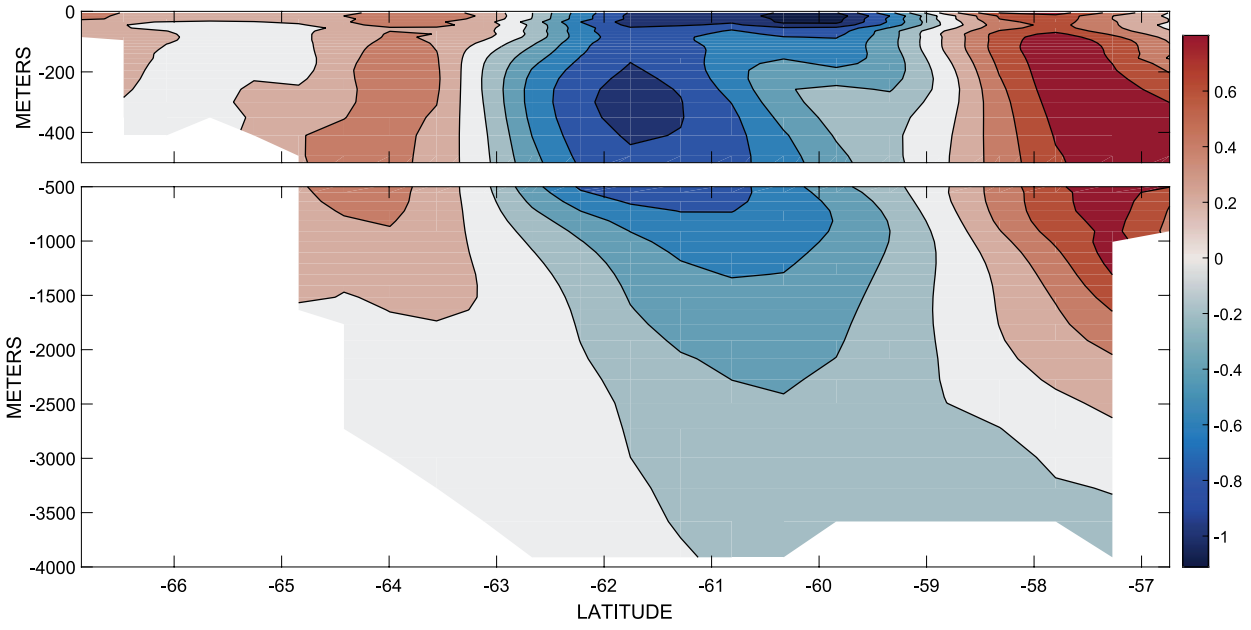


**Fig. 17. Anomaly of the zonal flow (cm $s^{-1}$) in the Drake Passage in 1995. Velocity as an annual average in this location proves very stable.**

(ECMWF) interim reanalysis (ERA-Interim; Dee et al. 2011, 2014) are among the prior estimates of the control variables. As is well known from a number of comparisons with other reanalysis products (e.g., Bromwich et al. 2007, 2016), none of these values can be regarded as very accurate. Chaudhuri et al. (2013, 2016) have discussed the errors that are assigned to them. In the process of determining the state estimate, these meteorological fields are adjusted so that the subsequent calculation with the free-running model, using the modified controls, renders it consistent with the ocean data. In general, the adjustments to the controls are small (see Fig. 19). A general result is a strengthening of the zonal winds in the regions of high-latitude westerlies and lower-latitude easterlies. The adjustments in $\tau_x$ are skewed toward positive values, while the meridional ones (not shown) are more symmetric and weaker.

The estimated wind stress along with the surface flows permits calculation of the rate of working of the wind on the ocean circulation. Because, like the heat and freshwater transports, it depends upon second-order products $\langle \mathbf{v} \cdot \tau \rangle$, only the map of $\langle u \rangle \langle \tau_x \rangle$ is displayed as an example (Fig. 20). Results such as these are an important part of the ongoing attempts to understand the oceanic circulation energy budgets (cf. Wunsch 1998; Zhai et al. 2012; Roquet et al. 2011).[2]

[2] A full discussion of the rates of wind work requires strong assumptions about the averaging interval chosen for values (hourly, monthly, annual, etc.).

*Mixed layer depth.* The oceanic mixed layer depth is a function both of the meteorology and oceanic dynamics. Using the Kara et al. (2000, 2003) definition based on density changes, Fig. 21 displays the 20-yr mean mixed layer depth. As expected (not shown), considerable seasonal changes exist in these values.

**DYNAMICS.** A full discussion of oceanic circulation dynamics is far beyond the intended scope of this overview. As an example, the Rossby number Ro = $UL/f$ is readily computed. At 722 m, with a fixed value of $L$ = 100 km the 20-yr average Ro are generally on the order of 0.001, except on the equator, and thus consistent with linear dynamics. Other Rossby number definitions can be used (e.g., from the vorticity field) and many other nondimensional parameters, such as Ekman and Reynolds numbers, can be computed.

Another example is shown in Fig. 22 as the 20-yr average angle between the ageostrophic component of the surface flow and the 20-yr average wind stress. With some exceptions, the estimated angle is not far from the canonical ±45°, changing sign across the equator. In the Southern Hemisphere, the most probable angle is −55°, and in the Northern Hemisphere it is 66°. The ageostrophic flow was calculated as the 5-m total flow minus the geostrophic component from the mean dynamic topography in Fig. 14. A number of assumptions go into the production of the conventional 45°, including accuracy of the stress estimate, having the true surface velocity, and the nature of the turbulence within the Ekman-like layer.

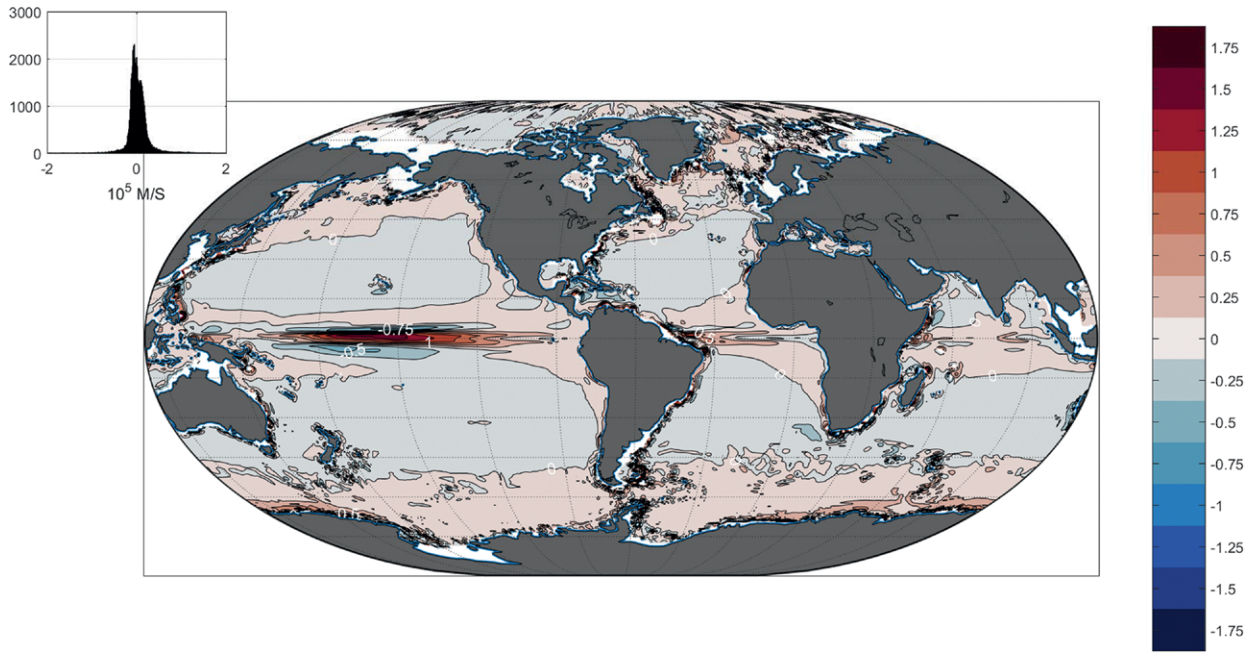


**Fig. 18. Twenty-year average vertical velocity ($10^5 w$) (m $s^{-1}$) at 105-m depth. This level is an approximate surrogate for the Ekman pumping velocity. The major gyres and equatorial upwelling are readily visible. See Liang et al. (2017b) for additional charts and discussion.**

Eddy physics, in the form of bolus velocities and vertical and horizontal mixing coefficients and viscosities, can also be discussed using state estimate products. These will be displayed and described more fully elsewhere.

**REGIONAL STUDIES.** Regional oceanographic subsets are easily extracted from the global files as time averages (annual, seasonal, etc.). A very large number of interesting regional studies is possible, bearing in mind the resolution problems near boundaries. As an example of what can be done regionally with salinity, Fig. 23 displays the 20-yr seasonal average anomalies at 5-m depth of salinity in the Bay of Bengal (see, e.g., special issue of *Oceanography*, 2016, Vol. 29, No. 2 for a comparison). Regional applications of the climatology

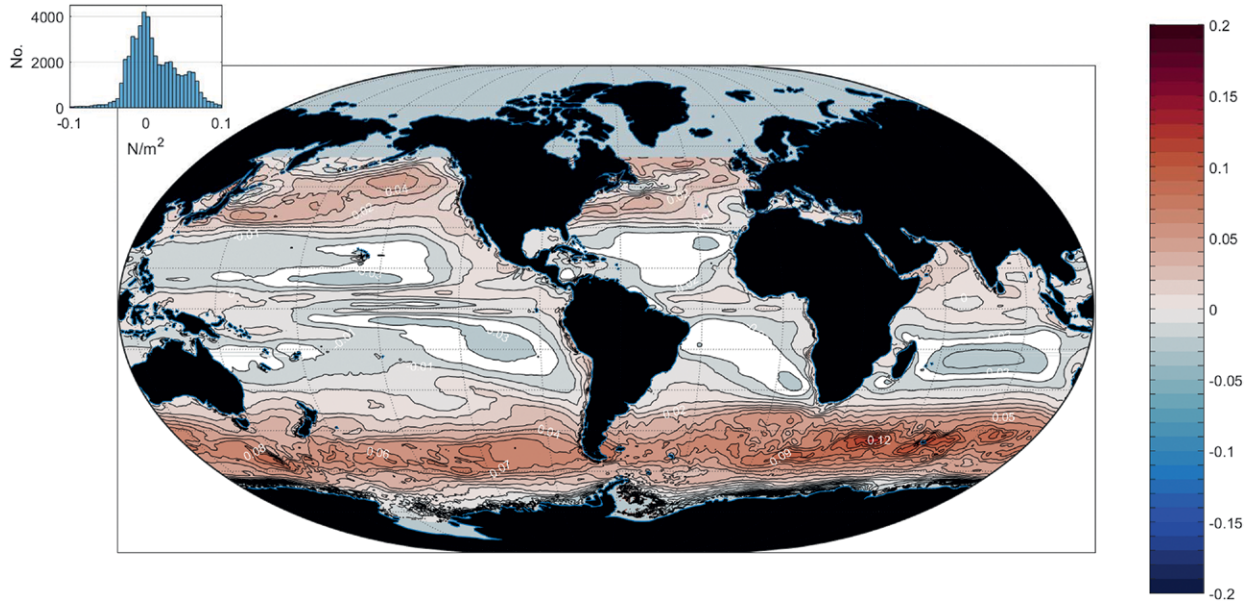


**Fig. 19. Adjustments made to the 20-yr average zonal wind stress $\tau_x$ (N $m^{-2}$). This chart can also be interpreted as the average misfit to ERA-Interim. Inset shows the histogram of adjustments, skewed positively.**

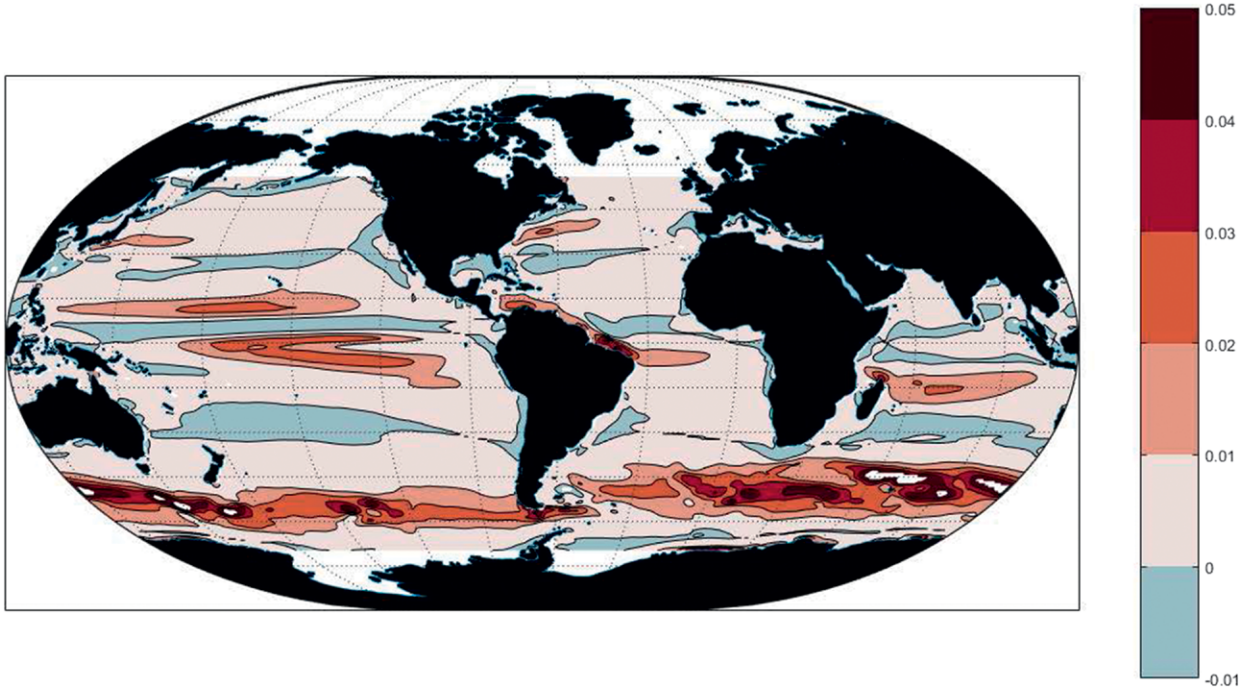


**Fig. 20. Rate of working of the time-mean zonal wind stress on the time-mean surface circulation (W m$^{-2}$). The quantitative importance of the Southern Ocean is apparent.**

can be seen in Wunsch and Heimbach (2013), Buckley et al. (2014, 2015), Evans et al. (2017), and Piecuch (2017)—all with a focus on the Atlantic Ocean.

**UNCERTAINTIES.** Determining uncertainties in results of "pure" data climatologies, data-constrained state estimates such as this one and in conventional unconstrained coupled or uncoupled models are a difficult problem for many reasons. These reasons range from model errors, to inadequate resolution, to a variety of problems connected with the observations. Boyer et al. (2016) discuss an upper-ocean 700-m climatology and separated the errors into those resulting from mapping methods and bias correction uncertainty, with methodology uncertainty dominating. A partial discussion of the uncertainties in the ECCO, version 4, estimate can be found in Wunsch (2018), where the stochastic error is separated, at least in part, from the systematic error. Thus, for example, the 20-yr global temperature is found to be 3.5127° ± 0.0014° ($2\sigma$) uncertainty with an approximate 20-yr mean heating rate of 0.48 ± 0.004 W m$^{-2}$ with uncertainties being the formal error derived from a bootstrap method. Paradoxically, it is only the short interval of 20 years relative to the far longer times required for the ocean to adjust on a large scale that justifies the assumptions leading to the error estimates. We also emphasize, once again, that quantities such as ocean temperatures and their changes (as in Fig. 8) reflect the implications of *all* the data, including those derived from meteorology and altimetry, not just the direct thermal measurements, as well as the information content lying with the space–time evolution of the dynamical model.

**FINAL REMARKS.** In brief, this 20-yr ocean climatology differs from those more conventionally available in a number of ways:

a) A large variety of near-global datasets combine to determine the state values. Each data type has specific error estimates, and all quantities calculated reflect the influence of all data types.
b) Data, beginning in 1992, although not entirely homogeneous over the 20-yr span, are nearly symmetric in distribution about the equator.
c) The values encompass the full water column and the entire ocean, including the Arctic regions.
d) All conventional output values of a general circulation model, including three components of velocity, pressure, temperature, salinity, sea ice, and their computable products (e.g., heat content change or the vorticity budget) plus mixing coefficients, are available, along with meteorological estimates dynamically consistent with the oceanic fields.
e) All basic conservation rules for the ocean circulation, including enthalpy and energy, are obeyed to machine precision in the model equations.

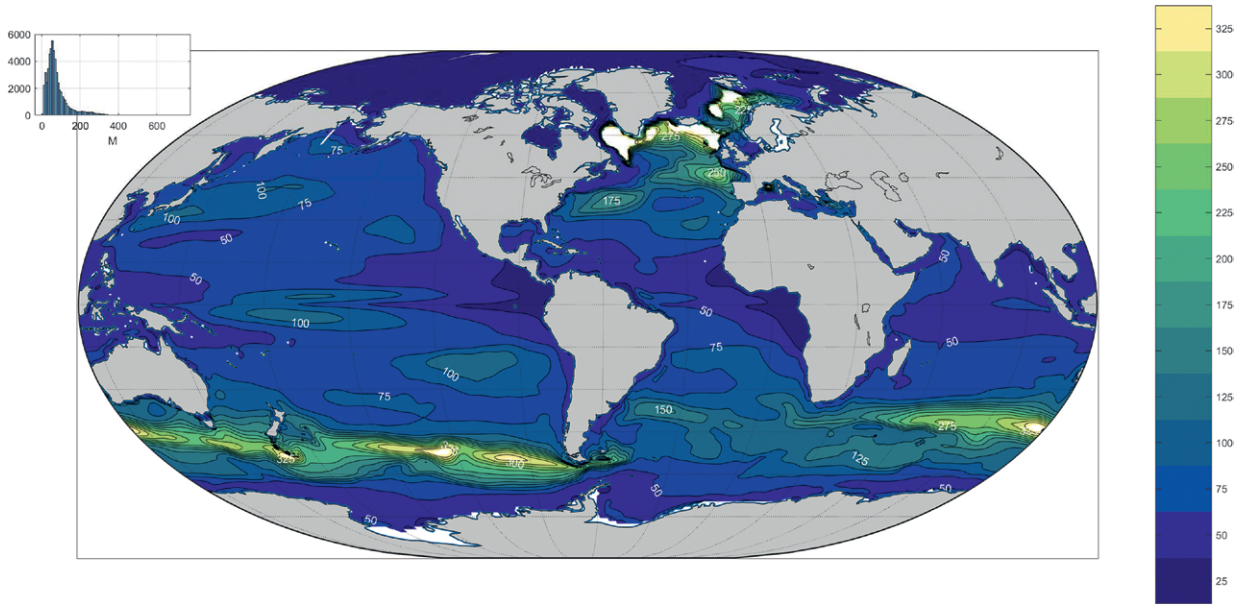


**Fig. 21. Twenty-year average mixed layer depth (m) as defined by Kara et al. (2003). Most of the ocean has values near 100 m, with extreme values above 700 m in the high-latitude North Atlantic Ocean and which are truncated here.**

Undoubtedly, a much longer averaging interval would produce quantitatively different results. A better (more accurate) estimate of the 20-yr period 1994–2013 is also surely possible, but the existing state estimate is arguably the best now available, and it permits a useful discussion of oceanic changes and their governing physics over two decades.

The gist of this paper is that understanding the ocean either as an instantaneous picture or as an average over any finite period must confront the intense time variability. Significantly improving the accuracy of future estimates, if interpreted as climatological averages, will not be easy, involving as it does the need for far longer records; much better observational

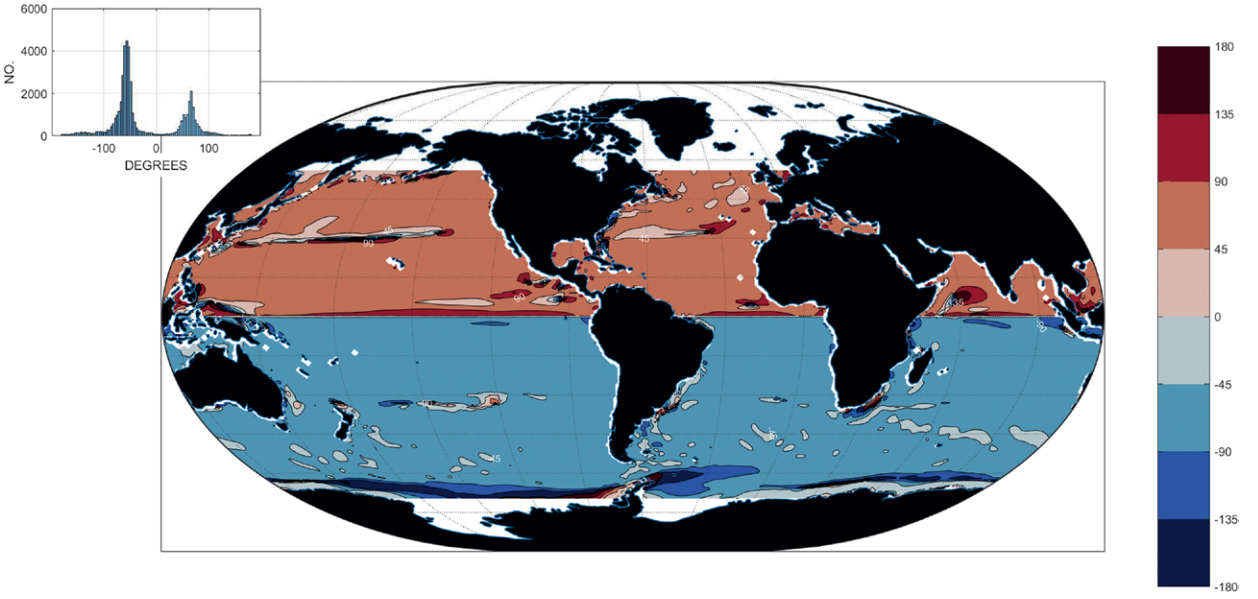


**Fig. 22. Angle (°) between the 20-yr average ageostrophic flow at 5 m and the 20-yr average adjusted wind stress. At the sea surface, a perfect Ekman layer would produce ±45° with the sign changing across the equator. Inset shows the bimodal histogram of angle values. Appearance of a near-classical Ekman layer becomes an important element in any discussion of the global ocean circulation, with many other components determinable from the ocean climatology results (overall vorticity balance, bottom boundary layer dissipation, etc.).**

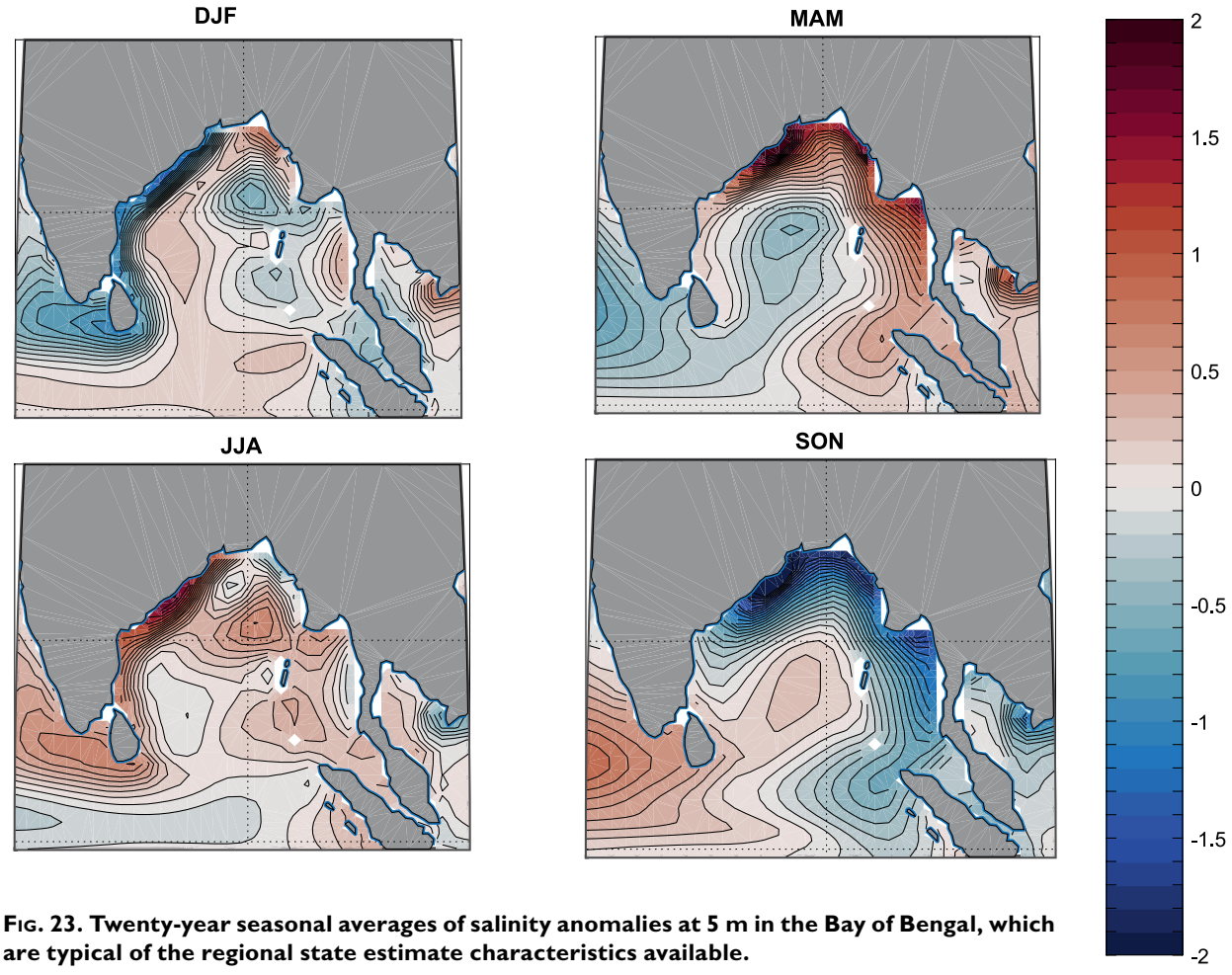


**Fig. 23. Twenty-year seasonal averages of salinity anomalies at 5 m in the Bay of Bengal, which are typical of the regional state estimate characteristics available.**

coverage of the ocean below 2,000 m; and, in specific regions, improved time–space resolution of both the observations and the underlying general circulation model. Better quantification of the error structures of all existing and future datasets is also very important.

**OBTAINING THE STATE ESTIMATE VALUES.** A concise documentation of ECCO, version 4, release 3, is given by Fukumori et al. (2017). The full state estimate values on the model native grid at monthly intervals from 1992 to 2015 are available online (at ftp://ecco.jpl.nasa.gov/Version4/Release3/) in Network Common Data Form (netCDF) form and include the full suite of data used in the least squares fitting. A subset of values making up the present climatology described here, 1994–2013, as described in ECCO Consortium (2017a,b) in MATLAB.mat files, can be found online (http://mit.ecco-group.org/opendap/diana/h8_i48/). Additional documentation is available that describes how to analyze property budgets using these estimates (Piecuch 2017) and how to run the model to produce additional fields not available in the archive (Wang 2017). Any of the authors can be contacted for help and advice. Comments about difficulties or errors are welcomed.

**ACKNOWLEDGMENTS.** ECCO has been funded over many years, primarily by the National Aeronautics and Space Administration at MIT, AER, JPL, and UT at Austin. The authors were supported in part through NASA Contract NNN12AA01C at JPL and NASA GRACE Grant NNH16CT00C at AER. Particular thanks are owed to NASA Program Manager Eric Lindstrom, for his sustained support and advice.

## REFERENCES

Abraham, J. P., and Coauthors, 2013: A review of global ocean temperature observations: Implications for ocean heat content estimates and climate change. *Rev. Geophys.*, **51**, 450–483, https://doi.org/10.1002/rog.20022.

AchutaRao, K. M., and Coauthors, 2007: Simulated and observed variability in ocean temperature and heat content. *Proc. Natl. Acad. Sci. USA*, **104**, 10 768–10 773, https://doi.org/10.1073/pnas.0611375104.

Adcroft, A., C. Hill, J.-M. Campin, J. Marshall, and P. Heimbach, 2004: Overview of the formulation and numerics of the MIT GCM. *Proceedings of the ECMWF Seminar on Developments in Numerical Methods for Atmospheric and Ocean Modelling*, ECMWF, 139–150, www.ecmwf.int/sites/default/files/elibrary/2004/7642-overview-formulation-and-numerics-mit-gcm.pdf.

Andersen, O., P. Knudsen, and L. Stenseng, 2015: The DTU13 MSS (mean sea surface) and MDT (mean dynamic topography) from 20 years of satellite altimetry. *IGFS 2014*, S. Jin and R. Barzaghi, Eds., International Association of Geodesy Symposia, Vol. 144, Springer, 111–121, https://doi.org/10.1007/1345_2015_182.

Bengtsson, L., S. Hagemann, and K. I. Hodges, 2004: Can climate trends be calculated from reanalysis data? *J. Geophys. Res.*, **109**, D11111, https://doi.org/10.1029/2004JD004536.

Boyer, T., and Coauthors, 2016: Sensitivity of global upper-ocean heat content estimates to mapping methods, XBT bias corrections, and baseline climatologies. *J. Climate*, **29**, 4817–4842, https://doi.org/10.1175/JCLI-D-15-0801.1.

Bromwich, D. H., R. L. Fogt, K. I. Hodges, and J. E. Walsh, 2007: A tropospheric assessment of the ERA-40, NCEP, and JRA-25 global reanalyses in the polar regions. *J. Geophys. Res.*, **112**, D10111, https://doi.org/10.1029/2006JD007859.

——, A. B. Wilson, L.-S. Bai, G. W. K. Moore, and P. Bauer, 2016: A comparison of the regional Arctic System Reanalysis and the global ERA-Interim Reanalysis for the Arctic. *Quart. J. Roy. Meteor. Soc.*, **142**, 644–658, https://doi.org/10.1002/qj.2527.

Buckley, M. W., R. M. Ponte, G. Forget, and P. Heimbach, 2014: Low-frequency SST and upper-ocean heat content variability in the North Atlantic. *J. Climate*, **27**, 4996–5018, https://doi.org/10.1175/JCLI-D-13-00316.1.

——, ——, ——, and ——, 2015: Determining the origins of advective heat transport convergence variability in the North Atlantic. *J. Climate*, **28**, 3943–3956, https://doi.org/10.1175/JCLI-D-14-00579.1.

Chaudhuri, A. H., R. M. Ponte, G. Forget, and P. Heimbach, 2013: A comparison of atmospheric reanalysis surface products over the ocean and implications for uncertainties in air–sea boundary forcing. *J. Climate*, **26**, 153–170, https://doi.org/10.1175/JCLI-D-12-00090.1.

——, ——, and ——, 2016: Impact of uncertainties in atmospheric boundary conditions on ocean model solutions. *Ocean Modell.*, **100**, 96–108, https://doi.org/10.1016/j.ocemod.2016.02.003.

Dee, D. P., and Coauthors, 2011: The ERA-Interim reanalysis: Configuration and performance of the data assimilation system. *Quart. J. Roy. Meteor. Soc.*, **137**, 553–597, https://doi.org/10.1002/qj.828.

——, M. Balmaseda, G. Balsamo, R. Engelen, A. J. Simmons, and J. N. Thépaut, 2014: Toward a consistent reanalysis of the climate system. *Bull. Amer. Meteor. Soc.*, **95**, 1235–1248, https://doi.org/10.1175/BAMS-D-13-00043.1.

ECCO Consortium, 2017a: A twenty-year dynamical oceanic climatology: 1994-2013. Part 1: Active scalar fields: Temperature, salinity, dynamic topography, mixed-layer depth, bottom pressure. Draft Version 1.2, MIT DSpace Rep., 54 pp., http://hdl.handle.net/1721.1/107613.

——, 2017b: A twenty-year dynamical oceanic climatology: 1994-2013. Part 2: Velocities, property transports, meteorological variables, mixing coefficients. Draft Version 1.3, MIT DSpace Rep., 45 pp., http://hdl.handle.net/1721.1/109847.

Evans, D. G., J. Toole, G. Forget, J. D. Zika, A. C. Naveira Garabato, A. J. G. Nurser, and L. Yu, 2017: Recent wind-driven variability in Atlantic water mass distribution and meridional overturning circulation. *J. Phys. Oceanogr.*, **47**, 633–647, https://doi.org/10.1175/JPO-D-16-0089.1.

Fenty, I., and P. Heimbach, 2013: Coupled sea ice–ocean-state estimation in the Labrador Sea and Baffin Bay. *J. Phys. Oceanogr.*, **43**, 884–904, https://doi.org/10.1175/JPO-D-12-065.1.

Forget, G., and R. M. Ponte, 2015: The partition of regional sea level variability. *Prog. Oceanogr.*, **137**, 173–195, https://doi.org/10.1016/j.pocean.2015.06.002.

——, J.-M. Campin, P. Heimbach, C. Hill, R. Ponte, and C. Wunsch, 2015: ECCO version 4: An integrated framework for non-linear inverse modeling and global ocean state estimation. *Geosci. Model Dev.*, **8**, 3071–3104, https://doi.org/10.5194/gmd-8-3071-2015.

Fu, L.-L., and E. A. Cazenave, 2001: *Satellite Altimetry and Earth Sciences: A Handbook of Techniques and Applications*. International Geophysics Series, Vol. 69, Academic Press, 463 pp.

Fukumori, I., O. Wang, I. Fenty, G. Forget, P. Heimbach, and R. M. Ponte, 2017: ECCO Version 4 Release 3. MIT DSpace Rep., 10 pp., http://hdl.handle.net/1721.1/110380.

Ganachaud, A., and C. Wunsch, 2000: Improved estimates of global ocean circulation, heat transport and mixing from hydrographic data. *Nature*, **408**, 453–457, https://doi.org/10.1038/35044048.

Gent, P. R., and J. C. McWilliams, 1990: Isopycnal mixing in ocean circulation models. *J. Phys. Oceanogr.*, **20**, 150–155, https://doi.org/10.1175/1520-0485(1990)020<0150:IMIOCM>2.0.CO;2.

Gouretski, V. V., and K. P. Koltermann, 2004: WOCE: Global Hydrographic Climatology. Bundesamt für Seeschifffahrt und Hydrographie Tech. Rep. 35/2004, 50 pp., www.bsh.de/de/Produkte/Buecher/Berichte_/Bericht35/Bericht1.pdf.

Ishii, M., M. Kimoto, and M. Kachi, 2003: Historical ocean subsurface temperature analysis with error estimates. *Mon. Wea. Rev.*, **131**, 51–73, https://doi.org/10.1175/1520-0493(2003)131<0051:HOSTAW>2.0.CO;2.

Kara, A. B., P. A. Rochford, and H. E. Hurlburt, 2000: An optimal definition for ocean mixed layer depth. *J. Geophys. Res.*, **105**, 16 803–16 821, https://doi.org/10.1029/2000JC900072.

——, ——, and ——, 2003: Mixed layer depth variability over the global ocean. *J. Geophys. Res.*, **108**, 3079, https://doi.org/10.1029/2000JC000736.

Kennedy, J. J., N. A. Rayner, R. O. Smith, D. E. Parker, and M. Saunby, 2011: Reassessing biases and other uncertainties in sea surface temperature observations measured in situ since 1850: 2. Biases and homogenization. *J. Geophys. Res.*, **116**, D14104, https://doi.org/10.1029/2010JD015220.

Knudsen, P., R. Bingham, O. Andersen, and M. H. Rio, 2011: A global mean dynamic topography and ocean circulation estimation using a preliminary GOCE gravity model. *J. Geod.*, **85**, 861–879, https://doi.org/10.1007/s00190-011-0485-8.

Koltermann, K. P., V. V. Gouretski, and K. Jancke, 2011: *Hydrographic Atlas of the World Ocean Circulation Experiment (WOCE). Volume 3: Atlantic Ocean*. M. Sparrow, P. Chapman, and J. Gould, Eds., WOCE Hydrographic Atlas Series, International WOCE Project Office, 221 pp.

Levitus, S., 1982*: Climatological Atlas of the World Ocean*. NOAA Prof. Paper 13, 173 pp. and 17 microfiche.

Liang, X., M. Spall, and C. Wunsch, 2017a: Global ocean vertical velocity from a dynamically consistent ocean state estimate. *J. Geophys. Res. Oceans*, **122**, 8208–8224, https://doi.org/10.1002/2017JC012985.

——, C. G. Piecuch, R. M. Ponte, G. Forget, C. Wunsch, and P. Heimbach, 2017b: Change of the global ocean vertical heat transport over 1993-2010. *J. Climate*, **30**, 5319–5327, https://doi.org/10.1175/JCLI-D-16-0569.1.

Locarnini, R. A., and Coauthors, 2013: *Temperature*. Vol. 1, *World Ocean Atlas 2013*, NOAA Atlas NESDIS 73, 40 pp.

Lumpkin, R., and K. Speer, 2007: Global ocean meridional overturning. *J. Phys. Oceanogr.*, **37**, 2550–2562, https://doi.org/10.1175/JPO3130.1.

Marshall, J., A. Adcroft, C. Hill, L. Perelman, and C. Heisey, 1997: A finite-volume, incompressible Navier Stokes model for studies of the ocean on parallel computers. *J. Geophys. Res.*, **102**, 5753–5766, https://doi.org/10.1029/96JC02775.

Maximenko, N., P. Niiler, L. Centurioni, M. Rio, O. Melnichenko, D. Chambers, V. Zlotnicki, and B. Galperin, 2009: Mean dynamic topography of the ocean derived from satellite and drifting buoy data using three different techniques. *J. Atmos. Oceanic Technol.*, **26**, 1910–1919, https://doi.org/10.1175/2009JTECHO672.1.

Medhaug, I., M. B. Stolpe, E. M. Fischer, and R. Knutti, 2017: Reconciling controversies about the "global warming hiatus." *Nature*, **545**, 41–47, https://doi.org/10.1038/nature22315.

Nguyen, A., V. Ocaña, V. Garg, P. Heimbach, J. M. Toole, R. A. Krishfield, C. M. Lee, and L. Rainville, 2017: On the benefit of current and future ALPS data for improving Arctic coupled ocean-sea ice state estimation. *Oceanography*, **30** (2), 69–73, https://doi.org/10.5670/oceanog.2017.223.

Ollitrault, M., and A. Colin de Verdière, 2014: The ocean general circulation near 1000-m depth. *J. Phys. Oceanogr.*, **44**, 384–409, https://doi.org/10.1175/JPO-D-13-030.1.

Piecuch, C. G., 2017: A note on evaluating budgets in ECCO Version 4 Release 3. NASA, 34 pp., ftp://ecco.jpl.nasa.gov/Version4/Release3/doc/evaluating_budgets_in_eccov4r3.pdf.

——, I. Fukumori, R. M. Ponte, and O. Wang, 2015: Vertical structure of ocean pressure variations with application to satellite-gravimetric observations. *J. Atmos. Oceanic Technol.*, **32**, 603–613, https://doi.org/10.1175/JTECH-D-14-00156.1.

Quinn, K. J., and R. M. Ponte, 2008: Estimating weights for the use of time-dependent gravity recovery and climate experiment data in constraining ocean models. *J. Geophys. Res.*, **113**, C12013, https://doi.org/10.1029/2008JC004903.

Reynolds, R. W., and T. M. Smith, 1994: Improved global sea surface temperature analyses using optimum interpolation. *J. Climate*, **7**, 929–948, https://doi.org/10.1175/1520-0442(1994)007<0929:IGSSTA>2.0.CO;2.

——, and ——, 1995: A high-resolution global sea surface climatology. *J. Climate*, **8**, 1571–1583, https://doi.org/10.1175/1520-0442(1995)008<1571:AHRGSS>2.0.CO;2.

Riser, S. C., and Coauthors, 2016: Fifteen years of ocean observations with the global Argo array. *Nat. Climate Change*, **6**, 145–153, https://doi.org/10.1038/nclimate2872.

Roemmich, D., and Coauthors, 2009: The Argo Program: Observing the global ocean with profiling

floats. *Oceanography*, **22** (2), 34–43, https://doi.org/10.5670/oceanog.2009.36.

Roquet, F., C. Wunsch, and G. Madec, 2011: On the patterns of wind-power input to the ocean circulation. *J. Phys. Oceanogr.*, **41**, 2328–2342, https://doi.org/10.1175/JPO-D-11-024.1.

——, and Coauthors, 2013: Estimates of the Southern Ocean general circulation improved by animal-borne instruments. *Geophys. Res. Lett.*, **40**, 6176–6180, https://doi.org/10.1002/2013GL058304.

Schlitzer, R., 2018: Ocean Data View Version 5.0.0. Alfred Wegener Institute, http://odv.awi.de.

Siedler, G., S. Griffies, J. Gould, and J. Church, 2013: *Ocean Circulation and Climate: A 21st Century Perspective*. 2nd ed. International Geophysics Series, Vol. 103, Academic Press, 904 pp.

Sonnewald, M., C. Wunsch, and P. Heimbach, 2018: Linear predictability: A sea surface height case study. *J. Climate*, **31**, 2599–2611, https://doi.org/10.1175/JCLI-D-17-0142.1.

Stammer, D., and Coauthors, 2002: Global ocean circulation during 1992–1997, estimated from ocean observations and a general circulation model. *J. Geophys. Res.*, **107**, 3118, https://doi.org/10.1029/2001JC000888.

——, and Coauthors, 2003: Volume, heat, and freshwater transports of the global ocean circulation 1993–2000, estimated from a general circulation model constrained by World Ocean Circulation Experiment (WOCE) data. *J. Geophys. Res.*, **108**, 3007, https://doi.org/10.1029/2001JC001115.

——, M. Balmaseda, P. Heimbach, A. Köhl, and A. Weaver, 2016: Ocean data assimilation in support of climate applications: Status and perspectives. *Annu. Rev. Mar. Sci.*, **8**, 491–518, https://doi.org/10.1146/annurev-marine-122414-034113.

Talley, L. D., and Coauthors, 2016: Changes in ocean heat, carbon content, and ventilation: A review of the first decade of GO-SHIP Global Repeat Hydrography. *Annu. Rev. Mar. Sci.*, **8**, 185–215, https://doi.org/10.1146/annurev-marine-052915-100829.

Thyng, K. M., C. A. Greene, R. D. Hetland, H. M. Zimmerle, and S. F. DiMarco, 2016: True colors of oceanography: Guidelines for effective and accurate colormap selection. *Oceanography*, **29** (3), 9–13, https://doi.org/10.5670/oceanog.2016.66.

Wang, O., 2017: Instructions for reproducing ECCO Version 4 Release 3. NASA, 6 pp., ftp://ecco.jpl.nasa.gov/Version4/Release3/doc/ECCOv4r3_reproduction.pdf.

Watkins, M. M., D. N. Wiese, D.-N. Yuan, C. Boening, and F. W. Landerer, 2015: Improved methods for observing Earth's time variable mass distribution with GRACE using spherical cap mascons. *J. Geophys. Res. Solid Earth*, **120**, 2648–2671, https://doi.org/10.1002/2014JB011547.

Wunsch, C., 1998: The work done by the wind on the oceanic general circulation. *J. Phys. Oceanogr.*, **28**, 2332–2340, https://doi.org/10.1175/1520-0485(1998)028<2332:TWDBTW>2.0.CO;2.

——, 2016: Global ocean integrals and means, with trend implications. *Ann. Rev. Mar. Sci.*, **8**, 1–33, https://doi.org/10.1146/annurev-marine-122414-034040.

——, 2018: Towards uncertainties in mean and changes in heat, salt, and surface elevation in the Global Ocean. *Tellus*, **70**, 1–14, https://doi.org/10.1080/16000870.2018.1471911.

——, and P. Heimbach, 2007: Practical global oceanic state estimation. *Physica D*, **230**, 197–208, https://doi.org/10.1016/j.physd.2006.09.040.

——, and ——, 2013: Dynamically and kinematically consistent global ocean circulation and ice state estimates. *Ocean Circulation and Climate: A 21st Century Perspective*, 2nd ed. J. C. G. Siedler, W. J. Gould, and S. M. Griffies, Eds., Academic Press, 553–579.

——, and ——, 2014: Bidecadal thermal changes in the abyssal ocean and the observational challenge. *J. Phys. Oceanogr.*, **44**, 2013–2030, https://doi.org/10.1175/JPO-D-13-096.1.

——, ——, R. M. Ponte, I. Fukumori, and ECCO Consortium Members, 2009: The global general circulation of the ocean estimated by the ECCO-Consortium. *Oceanography*, **22** (2), 88–103, https://doi.org/10.5670/oceanog.2009.41.

Zhai, X. M., H. L. Johnson, D. P. Marshall, and C. Wunsch, 2012: On the wind power input to the ocean general circulation. *J. Phys. Oceanogr.*, **42**, 1357–1365, https://doi.org/10.1175/JPO-D-12-09.1.